ELSEVIER

Journal of Power Sources 107 (2002) 245–272

JOURNAL OF POWER SOURCES

www.elsevier.com/locate/jpowsour

The European ALABC IMPLAB project: final results and conclusions

A. Cooper*

European Advanced Lead-Acid Battery Consortium (EALABC) (EEIG), 42 Weymouth Street, London W1G 6NP, UK

Received 31 August 2001; received in revised form 21 November 2001; accepted 7 December 2001

Abstract

This paper describes a project aimed at improving the performance and life of lead-acid batteries for electric vehicle applications and carried out by the European members of the Advanced Lead-Acid Battery Consortium. The project was divided into three principle tasks. The first concentrated on separator design and compression in order to improve cycle life. The second task sought to improve the specific energy of tubular plate designs, which traditionally have good life in traction applications. Additionally work was carried out to see the effects of rapid charging techniques on these improved designs. The third task sought to improve negative-plate performance by the characterization and evaluation of improved expanders. © 2002 Elsevier Science B.V. All rights reserved.

Keywords: Compression; Expanders; Fast charging; Lead-acid electric vehicle batteries; Separators; Tubular plates; Valve-regulated lead-acid batteries

1. Background

This project was designed to build upon the results achieved in project BE 7297 [1] during which, the following was shown.

- At the high rates of discharge experienced in EV applications, active material utilization is limited by acid availability rather than paste conductivity.
- Key factors in the improvement of cycle life of the valve-regulated lead-acid (VRLA) battery are: compression of the active mass by the separator, the construction of the absorptive glass mat separator and the nature of the charge regime employed to recharge the battery after use.
- It is possible to enhance considerably, the properties (strength and corrosion resistance) of the grid alloys used by additions of tin and silver.

Work elsewhere [2] has shown that rapid charging techniques, can improve cycle life of flat plate batteries apparently by modifying active material structure. Such techniques can however result in elevated temperatures in the battery and this can be detrimental to negative-plate life. Also such test regimes for EV batteries have demonstrated that the negative plate can fail under the influence of repeated, and prolonged, high-rate discharge pulses.

Accordingly the work in the present project focused on three areas.

1. Separator compression was studied across the plate stack as a whole in order to determine the reasons for the early initial loss of capacity experienced in these designs. Several different separator designs were studied with a view to overcoming problems of acid stratification and relaxation of compression during service. Some initial work utilizing ceramic separators was also included.
2. Improvement of the specific energy and life of lead-acid batteries with tubular positive plates was sought through the development of light-weight designs using the high-strength, corrosion resistant alloys mentioned above. In this type of battery, the positive active material (PAM) is constrained between the alloy spine and a porous fabric gauntlet, thus reducing opportunities for paste shedding on softening during cycling. Operating this type of battery under compression, in an AGM design, should help to maintain electronic conductivity within the active material, especially with the lower paste densities required for higher active material utilization. Rapid charging techniques have also been tried on these designs.
3. The mechanism of the degradation of the negative plate has been studied under conditions of electric vehicle service and work has been carried out to develop improved expander additives for the maintenance of the required open structure in the negative active mass.

2. Project structure and participants

The project participants were: Oldham France, Amer-Sil, Hollingsworth & Vose, The University of Kassel, ZSW

* Tel.: +44-207-499-8422; fax: +44-207-493-1555.
E-mail address: cooper@ldaint.org (A. Cooper).

0378-7753/02/$ – see front matter © 2002 Elsevier Science B.V. All rights reserved.
PII: S0378-7753(01)01076-X

(Ulm), Daramic, Sonnenschein, CMP Batteries, The Central Laboratory for Electrochemical Power Sources (Sofia), Digatron, Tudor (Spain) and The Politecnico di Torino.

The project was divided into three principal tasks, which are divided into smaller sub-tasks.

2.1. Separator design and compression

(a) A study of the effects of the compressive forces applied to the plate stack, using various AGM separator designs, on the cycle life of VRLA batteries.
(b) The evaluation of a novel type of separator on the performance and life of VRLA batteries.
(c) The evaluation of microporous ceramic materials for PAM constraint in high specific energy battery designs for electric vehicle applications.

2.2. Optimizing specific energy and performance of VRLA batteries utilizing novel, lightweight, tubular designs and high rate pulse charging techniques

(a) The construction and testing of optimized tubular and strap grid tubular (SGT) designs with thin plates.
(b) The influence of pulse charging techniques on the specific energy, life and charge time of advanced tubular designs.

2.3. Improvements in negative-plate performance

(a) Investigations into the degradation and performance of the negative plate arising from high rate discharge.
(b) A search for improved or synthetic materials for the negative plate.
(c) Improvement in the performance of the negative active mass through improved expanders.

3. Project results

3.1. Separator design and compression

3.1.1. Composite separators

Two novel types of separator were developed for incorporation into the test program, the first being a sandwich separator with the inner component made up of a special highly porous polymeric membrane surrounded by a 100% fine fiber AGM (proposal A). The second (proposal B) was made up of a multi-layered AGM separator with 100% fine fiber contacting the electrodes, whereas the inner part was made of a coarser fiber structure.

The cycling tests for the composite separator materials reached 750 cycles and Fig. 1 shows the evolution of the capacity for both types of separator. Some capacity loss after the first 50 cycles could still be observed for both proposals, but it was considerably less than seen on some previous ALABC tests.

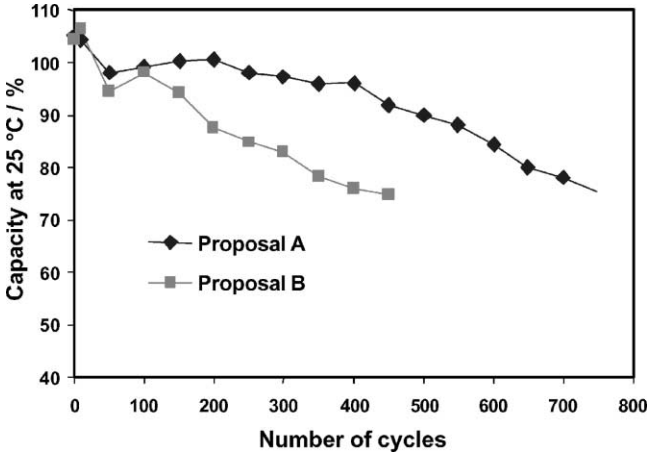

Fig. 1. Capacity evolution of the Amer-Sil proposal A and B cells.

With proposal B, two cells failed after 327 cycles, two others after 400 cycles and the remaining two cells only after 450 cycles. Bearing in mind the compression was only 35 kPa, the results obtained with proposal B (Fig. 1) can be considered satisfactory. This could be explained by the beneficial effect of the double layer of separator materials. With a specific surface area comparable to that of standard 100% glass single layer products (1.0–1.1 $m^2\,g^{-1}$), the separator design had been optimized in order to improve not only the wicking speed for easier filling (beneficial effect of the coarse layer), but also the saturation profile to achieve lower stratification (beneficial effect of the fine layer).

Proposal A showed an even better performance and maintained 90% of initial capacity up to 500 cycles. At this point, it was decided to remove two cells for analysis. The remaining four cells continued cycling and still had 84% of initial capacity at 600 cycles. Finally, three cells failed after 750 cycles.

The good results obtained with proposal A showed the beneficial effect of the microporous membrane sandwiched in between the two AGM layers made of 100% fine fibers. As the membrane was uncompressible, it allowed a good compression to be maintained in the battery. Its role was also to slow down the transfer of oxygen to the negative plate, allowing a more complete recharge of the plate before oxygen recombination took place.

Fig. 2 shows the overcharge factor during normal cycling compared to the overcharge factor during the capacity test for both proposals. The difference between the two factors is due to the different charging regimes, which were established as follows, prior to the start of the testing:

- during cycling: 7 h at $0.2C_5$ with a voltage limitation at 2.35 V and 1 h at $0.022C_5$ and
- for capacity test: 12 h at $0.2C_5$ up to 2.35 V and 3 h at $0.022C_5$.

During charge under normal cycling, both proposals behaved similarly with an overcharge factor of about 1.1.

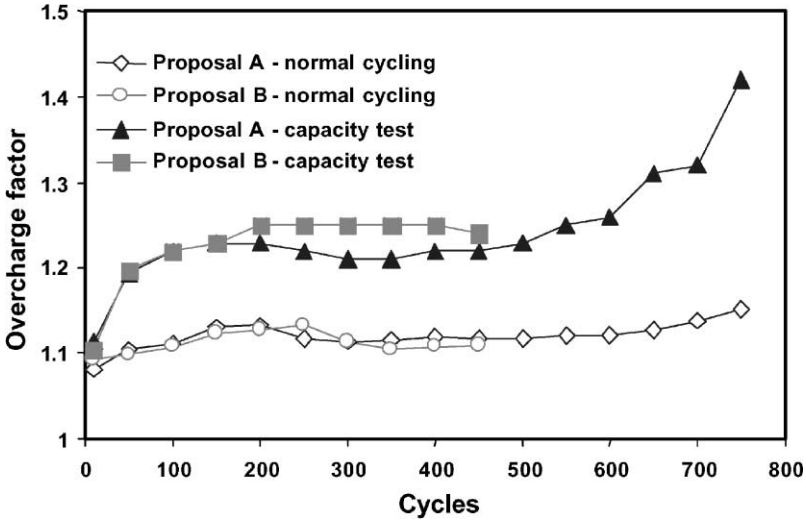

Fig. 2. Overcharge factors (during normal cycling and capacity test) for proposals A and B.

For the capacity tests, the overcharge factor was considerably higher.

For proposal A, the overcharge factor during capacity testing was stable during the first 450 cycles. From 450 to 600 cycles, the overcharge factor increased slightly, but the increase was more significant after 600 cycles. This corresponded exactly to the increase of the cells' weight loss and indicated that side reactions, like H_2 gassing, increased late in life and were detrimental to the charging process. The negative plate had been less and less charged, leading to the decrease of the capacity.

3.1.2. Separator blends

Two separator types were developed, being essentially blends of AGM and organic fibers. The two materials were labeled BGT 18423 (separator 1) and BGT 18449 (separator 2). These were built into cells for cycle testing. Full details of the construction of the test cells and early performance testing were given in the report presented at 8ABC [3]. The evolution of capacity of the various circuits is shown in Fig. 3.

Initially separator A (labeled circuit 5 in Fig. 3) failed at around 400 cycles, whereas in a repeat test the material completed 700 cycles to the 80% capacity mark. The cells were from the same batch yet one cycled for twice as long as the other.

The original test of separator B (circuit 6) failed at around 250 cycles, whilst the duplicate (circuit 3) performed erratically. It initially achieved 350 cycles to an 80% depth-of-discharge (DoD), but rebounded to give 700 cycles when left running.

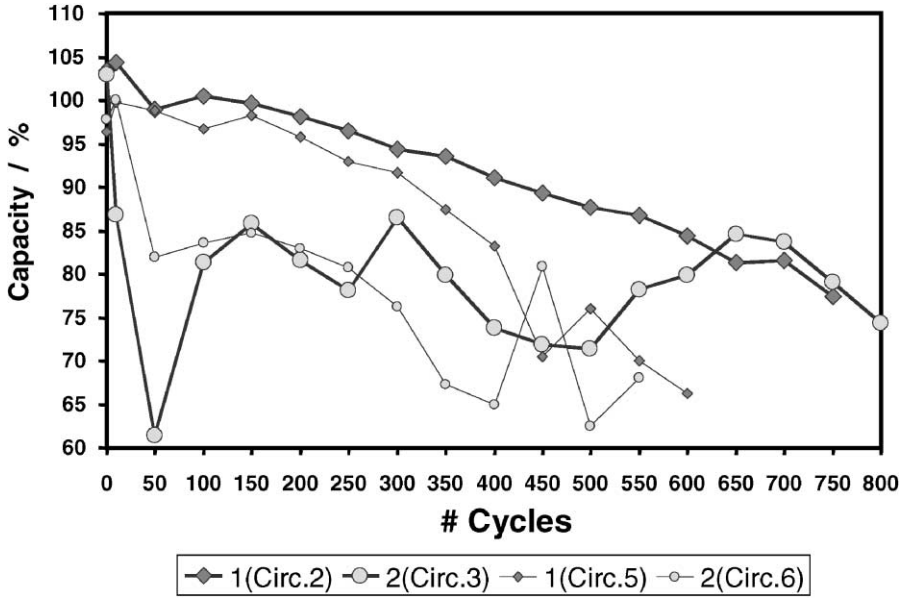

Fig. 3. Evolution of capacity of the H&V test circuits.

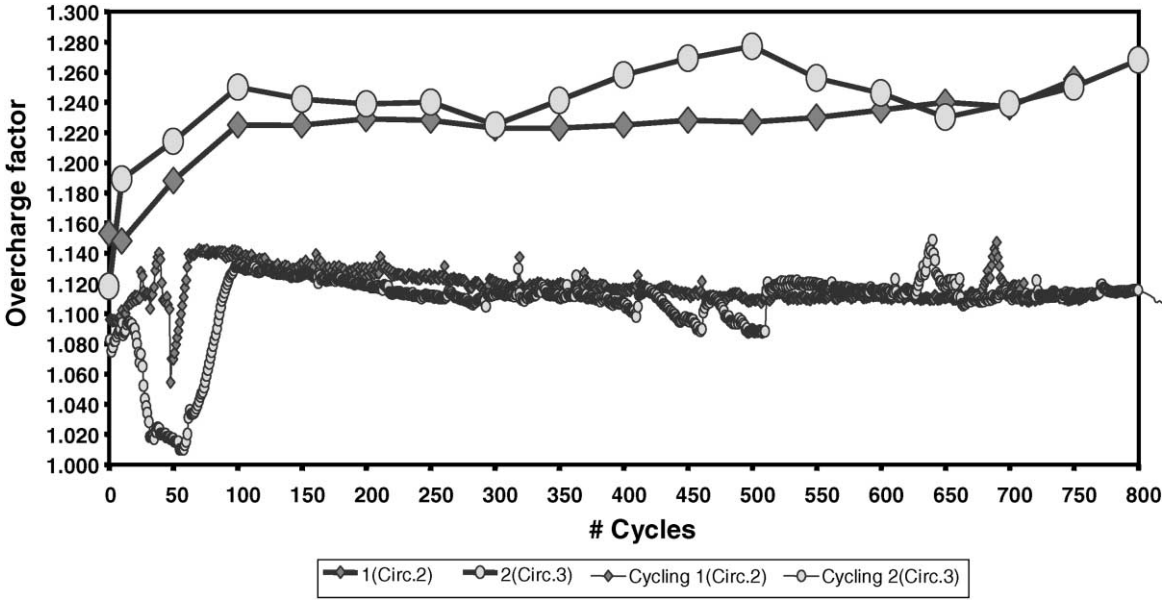

Fig. 4. Development of the overcharge factor during cycling of H&V separators.

The overcharge factors for these separators (Fig. 4) may give a clue as to the difference between the original and the replacement cells performances. With circuits 5 and 6, the initial 50 cycles were conducted with a very low overcharge and an equipment malfunction resulted in serious undercharging. The test equipment was checked, adjustments made and testing continued. The two repeat circuits (2 and 3) started with higher and more stable overcharge factors from the start and have maintained a more consistent trend. No abnormal problems were found in tear-down analysis and it was felt that all cells failed due to PAM degradation.

3.1.3. Oxygen transport tests

A purpose-designed rig was built to measure the rate of oxygen transport through candidate separator materials at several levels of saturation. These experiments are important, because there is now a feeling that oxygen transfer to the negative can inhibit charging of the negative plate and result in capacity decline.

The experimental set-up consisted of a sealed wicking rig with pairs of oxygen cells—one evolving and one consuming oxygen electrochemically. It allowed automatic and simultaneous monitoring of the electrical parameters of the electrochemical cells with time.

Five couples of oxygen-evolving and oxygen-sensor cells were positioned every 10 cm from 5 cm above the bottom of the rig. The oxygen sensor cell (OSC) consists of a zinc–air cell and a special design limits the current that can be drawn off the cell. This limiting current is a function of the oxygen partial pressure of the surrounding atmosphere. The oxygen-evolving cell (OEC) evolves oxygen under a constant current of 5 mA.

Fig. 5 shows the saturation of the electrolyte absorbed in the sealed wicking rig for the four separators tested in this project. Two of these separators, proposal B and BG 18423 are 50% filled with electrolyte only up to a height of 25 cm, whereas proposal A is filled to 40 cm. Separator BGT 18449 is starved of electrolyte (<50% saturation) at as low as 17 cm. Instead of electrolyte, there are voids in the pore systems of the separators that are filled with residual gas from the air, i.e. nitrogen and oxygen at the start and nitrogen alone after the OSCs have been switched on.

Fig. 6 shows the oxygen transport through the four separators, monitored as OSC currents at different height positions. The oxygen partial pressures monitored by the OSCs are very different for the different separators. The values are smaller in the higher positions. Fig. 6 shows that the proposal A separator and the H&V BG 18423 separator have similar values of the total OSC current at the greatest height, but quite a different distribution of the current values at lower positions within the rig.

These experiments have shown that three different regions in the separator can be identified.

(i) The area at the bottom (5–15 cm) which is completely filled with electrolyte. At this level, the proposal B separator and BGT 18449 show negligible transport of oxygen.
(ii) The area in the region between 15 and 25 cm, where all separators show maximum oxygen transport.
(iii) The area from 25 cm to the top of the rig. In this region, the amount of electrolyte absorbed in the pore system of the separators decreases rapidly and above 25–30 cm there is negligible electrolyte in the pores of the separator (apart from proposal A) and therefore no

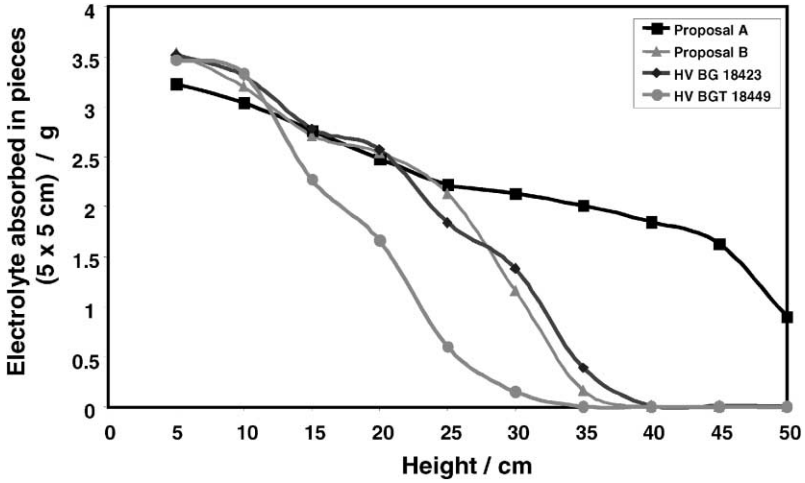

Fig. 5. Variation of saturation of the separators with height.

oxygen can be generated. This would suggest that the rig is unnecessarily tall for these experiments.

3.1.4. The evaluation of a novel type of separator (the acid-gellifying separator) on the performance and life of VRLA batteries

Samples of a new separator (AJS) were produced by Daramic with a high silica content and were characterized outside the battery. These results were reported at 8ABC [3]. Cycling tests on cells containing AJS, AGM and gel separator systems were carried out and the development of the C_2 capacity for the various cell types is shown in Fig. 7. The C_5 capacity is shown in Fig. 8.

The best life-capacity result was obtained for the AJS cell under 80 kPa initial external mechanical pressure, although the gel cell performed at higher capacity until it failed after about 400 cycles. The AJS cell containing phosphoric acid subjected to 80 kPa also shows a good sustained capacity. The capacities of cells with the higher levels of compression were sustained at higher levels than those with low compression.

The charge factor related to the C_2 cycles is shown in Fig. 9. It appears that there were short circuits in the gel cell (after about 400 cycles), and in the AJS 80 kPa cell (after about 1000 cycles. At the start of cycle life, the charging regime was adjusted many times in order to obtain a charge factor in an acceptable range (i.e. over 1.05). In particular, the constant voltage charging phase was limited to 2.4 V/cell, which proved to be too low for the AJS systems and also for the gel cell. Table 1 shows the charging regimes for the different cells at all stages in the cycle life test.

Since no experience existed previously, these tests resulted in the development of an optimum charging regime for the new separator systems. It transpired that the new AJS system requires a charging voltage comparable with that for the gel system and the flooded systems. Therefore, in a subsequent test on batteries and on new cells, a high

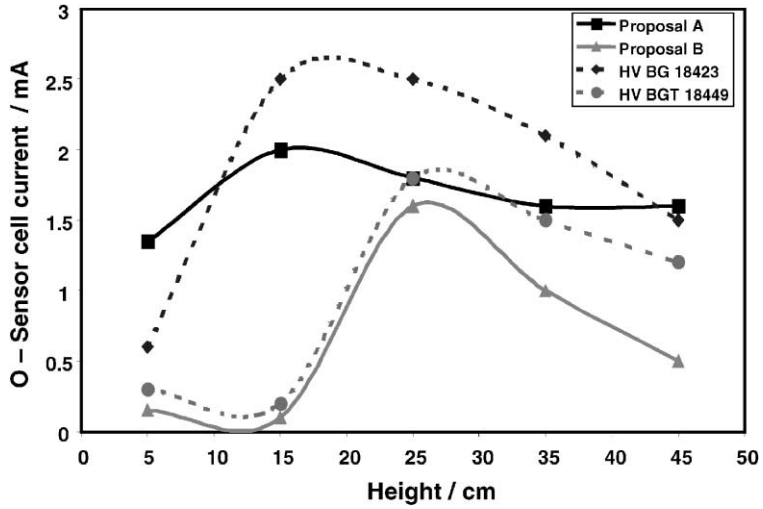

Fig. 6. Oxygen transport of the different AGM separators in the rig.

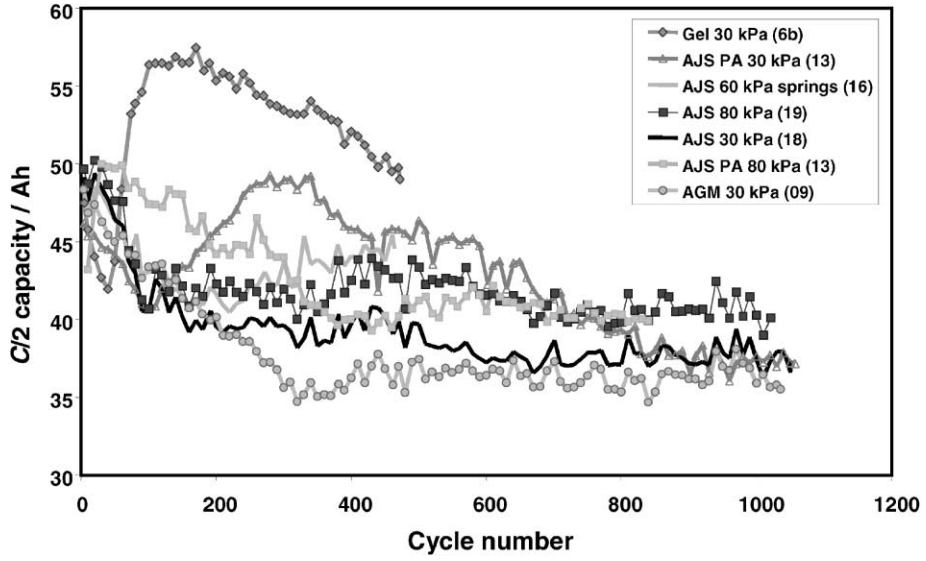

Fig. 7. Evolution of the C_2 capacity of the initial cells vs. cycle number.

charging voltage (2.45 V/cell) and a constant current period at the end of charge were integrated into the charging regimes.

The tests on the original cells have shown that the AJS cells perform best under 80 kPa initial mechanical pressure. The addition of phosphoric acid to the electrolyte seems to lead to a reduction in corrosion of the positive plate but at the same time, the standard AJS was oxidized to a depth of some microns on the side in contact with the positive plate. The corrosion product was a white silica oxide layer without any detrimental influence on the cell behaviour.

A group of 12 V, 48 Ah batteries was built by Sonnenschein, all with the same plate design but with different separator systems and corresponding acid contents. The AJS batteries were 100% saturated while, in the AGM versions, somewhat more electrolyte was added than in the original cells (95% saturation). The evolution of the relative capacity for the batteries made up with the various separation systems is shown in Fig. 10.

Once more a gel variant (this time maintained at constant thickness) showed the highest capacity for 400 cycles, but then failed. Only the AJS batteries showed a long-term stable behaviour, with the one subjected to the highest initial mechanical pressure having the best cycling life (about 500 cycles to 80% of the initial capacity).

While the capacity of AJS battery subjected to 60 kPa initial pressure dropped to the 80% level around cycle 130, a slower decrease of capacity was observed for the battery set under 80 kPa initial pressure. The cell performed 510 cycles

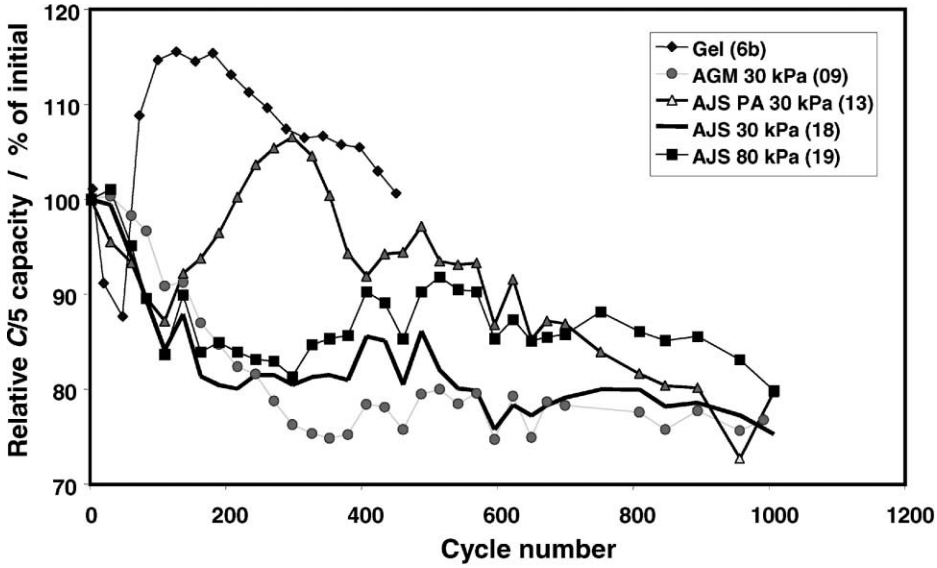

Fig. 8. Evolution of the C_5 capacity of the initial cells vs. cycle number.

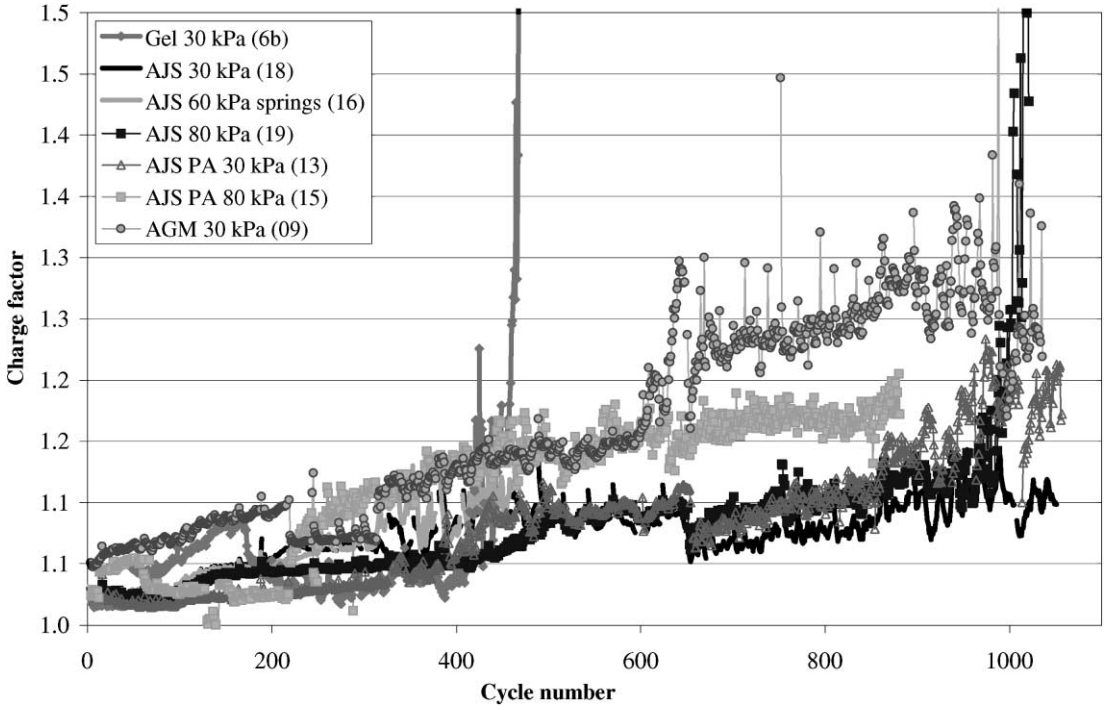

Fig. 9. Evolution of the charge factor of the initial cells vs. cycle number.

before falling below the 80% criterion. As the grids are from the same production as for those of the other battery types, it is interesting that the other batteries finished their life because of corrosion and those with the AJS separator still have a steady capacity (even if the capacity is already below the end of life criterion).

In summary, the long life obtained with the first batch of cells was not completely matched by the batteries. Although lower cycle lives than expected were obtained, the AJS units again performed in the most stable fashion. In the same way, for each type of battery, the sample subjected to an external mechanical pressure performed the best. It was also proved that the application of mechanical pressure leads to a lower corrosion of the grids.

The principal conclusions of this part of the program are as follows.

- The utilization of AJS in combination with the application of external mechanical pressure leads to over 1000 full C_2 cycles in a cell and over 500 cycles in a battery.
- The life limiting factor for the cells was probably the corrosion of the positive grids while for the batteries, the progressive decrease in capacity is probably attributable to a compaction of the negative active material (NAM).
- The application of mechanical pressure reduces the positive grid corrosion—the higher the mechanical pressure, the lower the corrosion.

3.1.5. The evaluation of microporous ceramic separators for positive active material restraint in high specific energy battery designs for electric vehicle applications

It has been shown elsewhere in the ALABC research program [4] that compression of the positive active mass is a

Table 1
Charging regimes of the initial cells and the modifications

Cycle	AGM	AJS 80 kPa	AJS PA 30 kPa	AJS 30 kPa	AJS 80 kPa springs	Gel
1			14.4 A/2.4 V/10 h			14.4 A/2.45 V/10 h
47						14.4 A/2.45 V/6 h
61						400 mA/4 h
102				14.4 A/2.45 V/10 h		
172						14.4 A/2.4 V/10 h
220	14.4 A/2.35 V/10 h					
232				14.4 A/2.4 V/10 h		
265					14.4 A/2.4 V/10 h	
313						14.4 A/2.45 V/10 h
316	14.4 A/2.4 V/10 h					

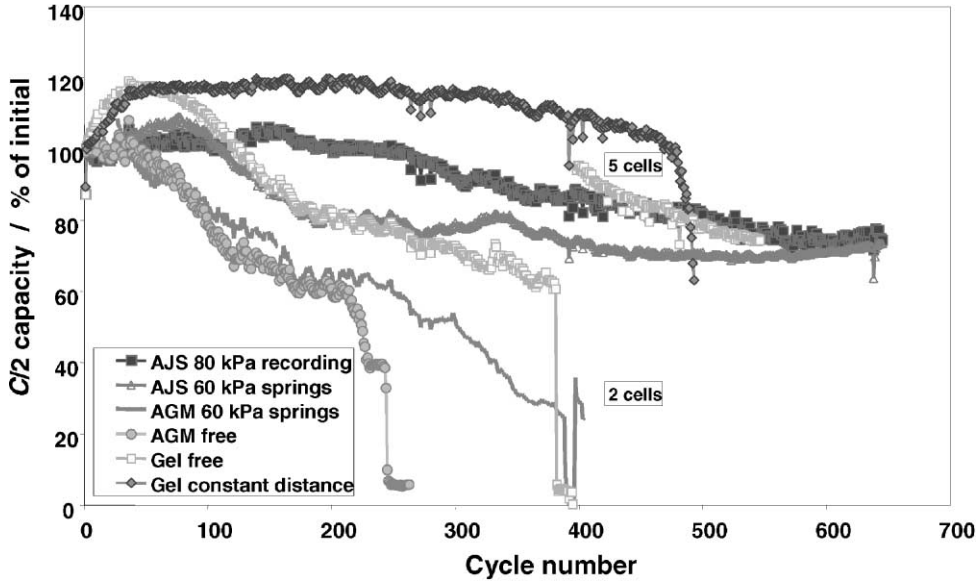

Fig. 10. Evolution of the relative C_2 capacity with the cycle number for the batteries.

key factor in battery life under deep cycling conditions. This should be one of the functions of the separator. However, there is evidence that with the conventional glass mat separators, the compression characteristics are adversely affected once they have been compressed during assembly of the battery and also with addition of the acid. A rigid separator, in the form of a microporous ceramic material, was tested in the hope that this relaxation could be avoided and thus provide better compression on the active material.

Two grades of ceramic material were evaluated in 8 V cells cycled with 1.25 A discharge current down to 1.5 V per cell (100% DoD). *IU* charging (15 h) was used with $I = 1$A and $U = 2.4$ V per cell. However the capacity fell markedly within 100 cycles for both variants (Fig. 11). It was concluded that the pore size of the material was too large and this allowed the development of short circuits, and the penetration of the open porosity by the active material as it swelled with cycling.

3.2. Design, construction and testing of optimized tubular and strap grid tubular batteries with thin plates

Lead-acid batteries with tubular positive plates have long cycle lives but, high rate performance for EV applications, has been limited by the limitations which relatively large plate couple pitch impose on impedance and plate current density. Performance improvements have been pursued through the development of thin tubular positive plate technologies.

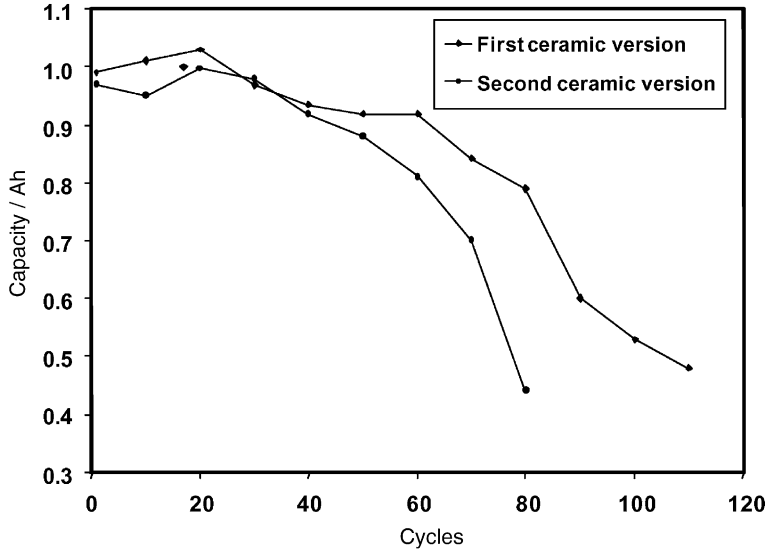

Fig. 11. Cycle test at a discharge rate of 1.25 A (100% DoD) of 8 V batteries with the first and second versions of the ceramic separators.

3.2.1. Fine spine tubular positive plate designs

A matrix of process and design variables was explored and test cells and batteries were manufactured at CMP Ltd. The best performing variant, using the 13-plate design with thinner plates, yielded an ECE-15L specific energy of 29 Wh kg^{-1}, representing a 60% improvement over that of existing tubular products and within the performance range of pasted plate valve-regulated batteries.

The progressive enhancement of ECE-15L performance is illustrated, for the evolving design, in Fig. 12. Discharge curves are presented for cells based on existing technology and the two development designs. Improvement of specific energy follows from a higher discharge voltage as well as from extended discharge duration. Life tests of cells were made at 35 °C, charging with an *IUI* characteristic with the initial stages limited at 20% C_5 A and 2.35 V and continued charge at 1.6% C_5 A to an overcharge of 4% C_5. The results are shown in Fig. 13.

Following removal of the discharged stand period of 1 h at cycle 9, the specific energy appeared stable for successive cycles until it fell below 75% at cycle 48. Following a 5 h rate measured discharge, specific energy recovered and remained stable until it fell below 75% at 67 cycles. Cycle testing continued with the initial rate of charge increased

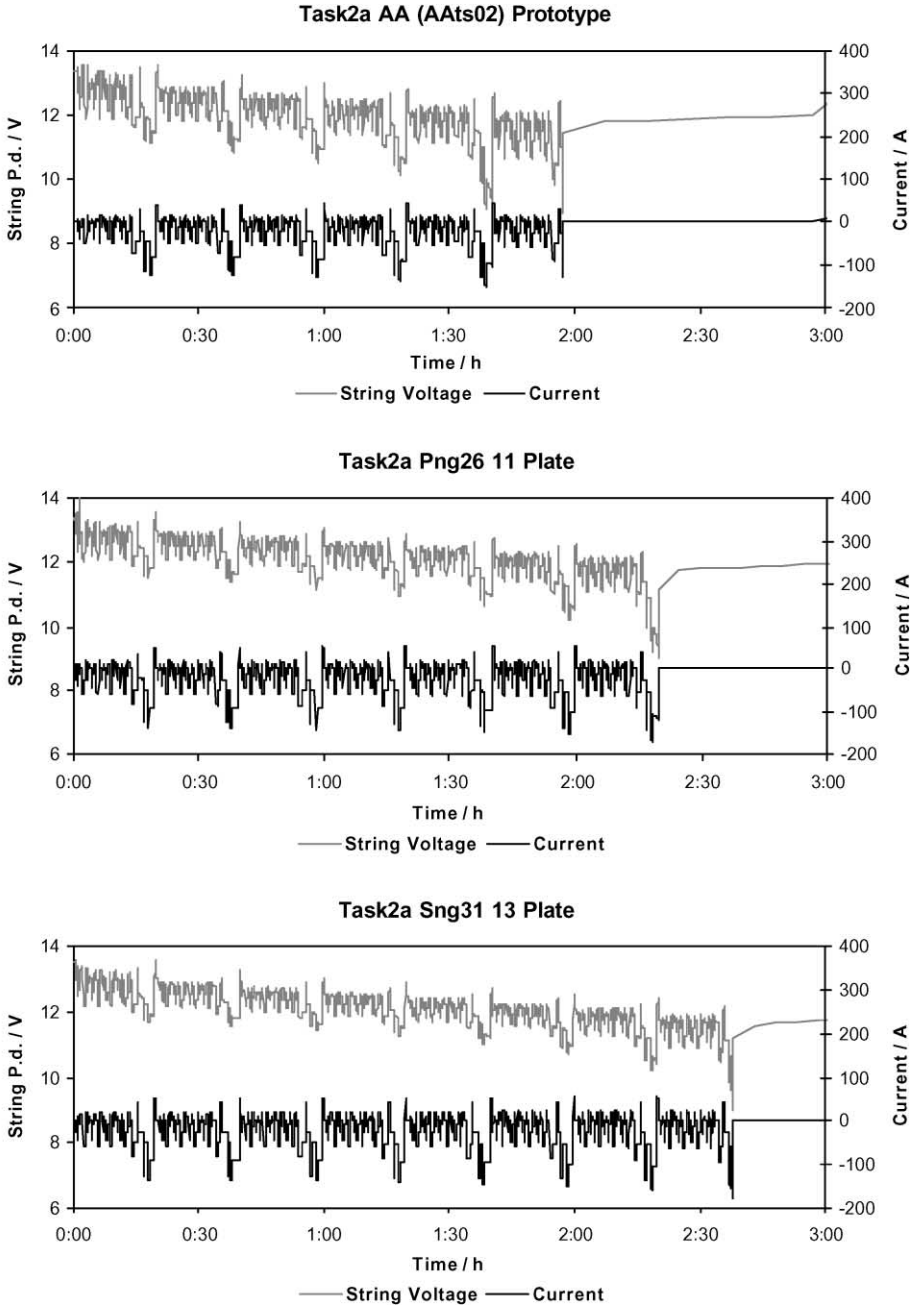

Fig. 12. Progressive enhancement of ECE-15L performance with design.

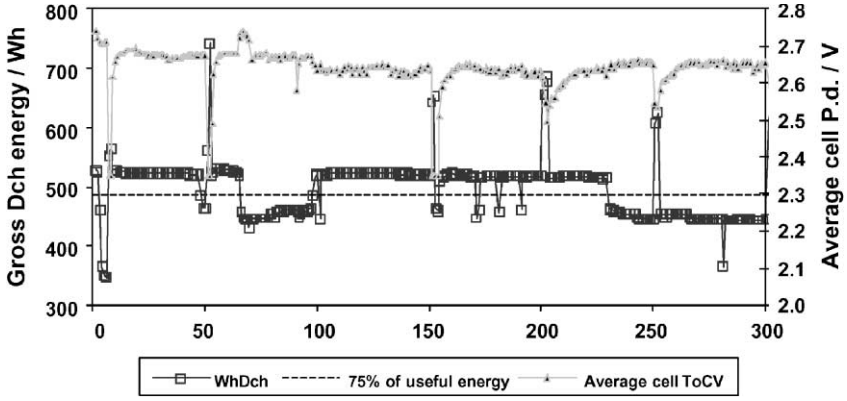

Fig. 13. ECE-15L cycling with thinner-plate cells.

from 20 to 40% C_5 at cycle 76. Specific energy increased to greater than 75% at cycle 100 and remained relatively stable until it declined again after a total of 230 cycles.

Mass/water loss amounted to 55 g/cell for all conditioning and characterization tests and the first 50 cycles and an additional 35 g/cell to cycle 300. Batteries of the preferred design were made and commissioned but initial performance was variable and low in comparison with the prototype cells. Initial performance of the best batteries approached expectations based on prototype cell performance but there appeared to be a problem with sustaining ECE-15L 80% cycle performance. Diagnostic tests indicated that positive plate performance was reduced in a manner that is reminiscent of thermopassivation. The problem may follow from extended in-process storage of components or process conditions that were different for the cell and battery components.

Variable poor performance of batteries is due to positive plate performance. The over-discharge characteristics are reminiscent of diode-like polarization that is associated with thermopassivation. It is conceivable that the process conditions that would promote thermopassivation could render electrodes vulnerable to an equivalent condition of premature capacity loss. Poor performance in another ALABC project (ALABC A005-3) was attributed to extended storage of formed and poorly dried positive plates. While the CMP plates suffered processing delays, incomplete drying is not suspected. Cells that had consistently good performance had laboratory-processed components.

3.2.2. Strap grid tubular plate designs

The basic objective of this part of the program was to study the changes in the structure of the PAM in VRLA batteries during ECE-15 cycling and to improve the performance of the positive plates used in VRLA batteries for EV applications by creating a technology for production of SGT plates with an optimum PAM structure.

It was established that two layers are formed in the positive active mass. One layer is in contact with the corrosion layer and collects the current from the PAM and conducts it to the active mass collecting layer (AMCL), and another external PAM layer, actually determines the capacity of the plate (external working layer of the active mass: EWLAM). On battery cycling, the AMC layer becomes powdery and often loses contact with the EWLAM layer. Consequently, parts of the outer PAM layer are excluded from the current generation and accumulation processes and the capacity of the plate declines. The formation of this brittle PAM layer is probably due to some restriction in the H_2SO_4 flow through the PAM, which changes the pH of the solution in the pores.

A series of SGTP batteries was subjected to cycling tests according to the requirements of European ECE-15L test protocol for EV batteries. The batteries under test have endured 950 ECE-15L cycles, which corresponds to a distance run of about 48,000 km. The tear-down analysis of this battery showed that its life had been limited by corrosion of the straps of one of the positive plates. The test results also indicate that the plates with PAM density $d = 4.60$ g cm^{-3} have the best cycle life performance. It has further been established that, in order to ensure long cycle life of the battery and high capacity performance in its middle life period, the charge current should be higher than $1.5C_5$ and the voltage should not exceed 15.30 V.

Another battery, labeled BS4, was subjected to cycling tests following the ECE-15 profile for hybrid electric vehicle batteries in order to investigate the effect of battery charge mode on its energy performance. During the cycling test the peak power in the first three ECE-15 cycles before the charge generator was switched on was measured. Fig. 14 presents the peak power values as a function of the number of cycles. P_1 denotes the power delivered at the maximum charge current during the first ECE-15 cycle, P_2 stands for the power output during the second ECE-15 cycle and P_3, during the third ECE-15 cycle prior to switching on the generator.

Until cycle 400 (zone A), the charge algorithm included galvanostatic charge at $I = 0.4$ C until a charge voltage of 15.0 V was reached, followed by charge at 15.0 V up to a charge factor 108%. After the first 100 cycles, the power

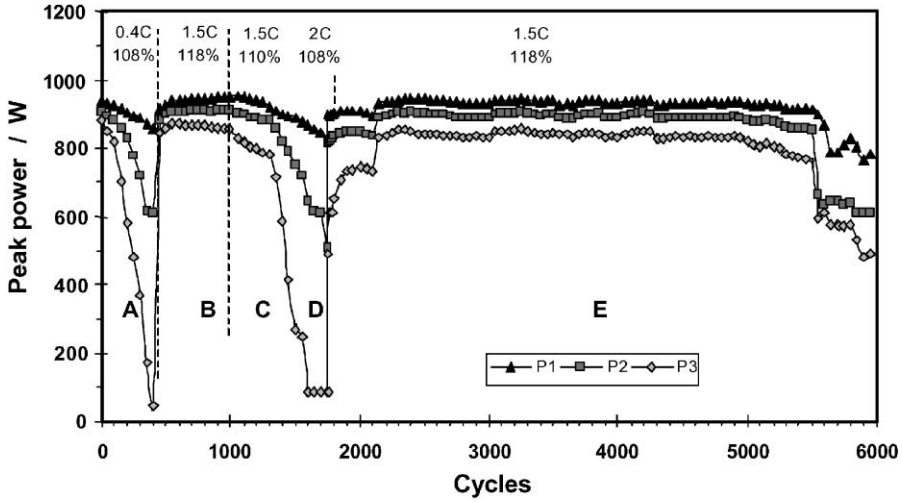

Fig. 14. Peak power changes on cycling of battery BS4.

output began to decrease reaching a cut-off-peak power of 550 W after 200 cycles. After the 400th cycle, the charge algorithm was changed to a new one: $I_1U_2I_3$, where $I_1 = 1.5C_5$, $U_2 = 15.2$ V and $I_3 = 0.1C_5$ up to a charge factor of 118% (zone B). Under this charge mode, the battery was restored completely (during all three ECE-15 cycles) to its initial power output of about 900 W and preserved this power performance for more than 550 cycles. After that, during cycle 1000, the third step comprising galvanostatic charge ($I_3 = 0.1C_5$) was excluded and the charge was completed at a charge factor of 108%. This change in the charge algorithm leads to a slow decrease in battery power output during the second and third ECE-15 cycles (zone C). Then, at the 1150th cycle, the charge factor was increased to 110%, but no increase in power output was observed. In order to check the influence of charge current on the state of charge of the battery, it was increased to $I_1 = 2.0C_5$ and the charge factor was reduced to 108% (zone D). Under this charging mode an abrupt decline in power output was registered, the power reaching almost zero at the third ECE cycle. Then the charge mode applied in zone B was used again ($I_1U_2I_3$, where $I_1 = 1.5C_5$, $U_2 = 15.2$ V and $I_3 = 0.1C_5$ up to a charge factor of 118%) (zone E). As evident from the figure, the battery restored its high power output, especially after addition of water at the 2100th cycle, and these high power values were maintained for more than 3700 cycles. As evident from the figure, the life of the battery was 5500 hybrid cycles, which corresponds to a distance run of about 60,000 km. It should be noted that these charge modes required the addition of 20 ml of water to each of the cells every 500 cycles.

It was established that structural changes in the PAM limited the cycle life of the battery. There were no signs of serious corrosion of the straps and the latter could endure many more charge–discharge cycles.

The tests performed with SGT plates with different active mass densities have shown that battery cycle life can be improved by increasing the PAM density to 4.60 g cm^{-3}. In order to preserve the good power performance of the SGT plates on increasing the PAM density, the thickness of these plates should be reduced. In earlier examples, the thickness of the SGTP plates was 5 mm with a 2 mm PAM layer on both sides of the strap grids. A new thinner SGTP plate (3 mm) was developed by CLEPS with a 1 mm PAM layer on both sides of the strap grid. This new SGTP design is presented schematically in Fig. 15.

The 4BS paste was produced and was diluted to a suspension with a density of 1.80 g cm^{-3}, which was filled (under a pressure of 4 atm) into die-cut SGT plates (3 mm thick).

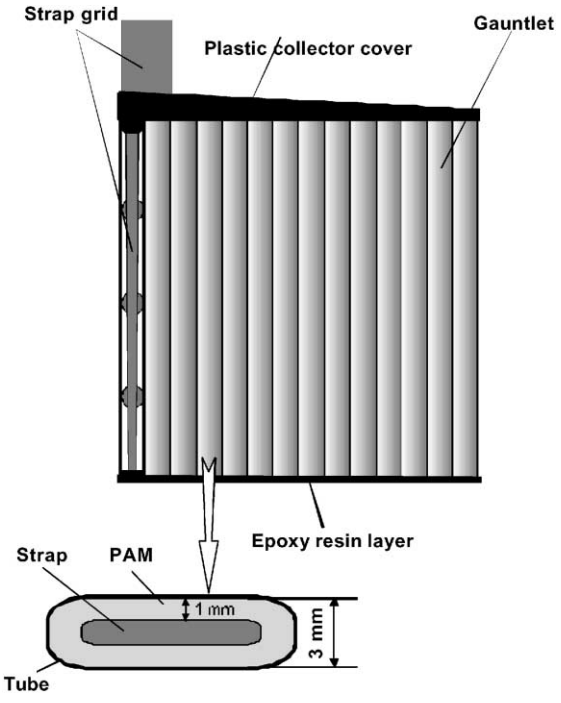

Fig. 15. A drawing of the 3 mm SGTP.

Table 2
Battery characteristics

Battery type	Die-cut SGTP (3 mm)
Amount of PAM (g cell)	420
PAM density (g cm^{-3})	4.65
Amount of NAM (g cell)	410
PAM utilization (g Ah)	13.2
NAM utilization (g Ah)	12.8
H_2SO_4 amount (g cell)	480

The strap grids were die-cut from a Pb–Ca–Sn sheet (1 mm thick), supplied by Cominco (Canada). These plates were then cured.

The negative paste contained a blend of 0.15% Indulin (In) + 0.08% Vanisperse A (VAN) as the expander. This was pasted over negative grids of the SLI type, which were also cured. Then the positive SGTP and the negative plates were formed in H_2SO_4 solution of 1.15 g cm^{-3} and assembled into batteries with two SGTP and three negative plates per cell. An AGM (H&V) separator was used at 30% compression. The basic characteristics of these batteries are summarized in Table 2, where the PAM and NAM coefficients are given for 2-h rate of discharge.

One of these batteries (BC8) was subjected to the ECE-15 cycling test according to the requirements for hybrid electric vehicles. The battery was charged employing the following algorithm: $I_1U_2I_3$

$I_1 = 1.5C_5$ up to $U_2 = 15.25\,\text{V}$

$U_2 = 15.25\,\text{V}$ until $F_{\text{ch}} = 108\%$

$I_3 = 0.1C_5$ until $F_{\text{ch}} = 118\%$

During the first few cycles, the internal resistance of the battery was measured. Fig. 16 shows the dependence of the internal resistance at high current power on the DoD for battery BC8 (3 mm). These results are compared with the data obtained in 1999 for the internal resistance of battery BC4 (5 mm).

As is evident from the figure, both batteries have a very similar internal resistance on discharge, which implies that the expected increase in internal resistance as a result of increased PAM density is compensated for by the reduced PAM thickness.

This battery was subjected to ECE-15 cycling tests for hybrid electric vehicle applications using the following charge algorithm:

$I_1 = 1.5C_5$ up to $U_2 = 15.25\,\text{V}$

$U_2 = 15.25\,\text{V}$ until $F_{\text{ch}} = 108\%$

$I_3 = 0.1C_5$ until $F_{\text{ch}} = 118\%$

The results obtained are presented in Fig. 17.

The battery with 3 mm plates exhibited a life of 4000 hybrid cycles when the optimum charge algorithm was employed. This cycle life is a bit shorter than that of the battery with 5 mm plates.

On completion of the cycling tests all battery cells were dismantled and autopsied. It was established that the negative plates were in good condition with no visible swelling of the active mass. The positive plates were visibly in good condition. Only one plate (out of 18) had straps interrupted by corrosion in their upper part close to the top bar. The other 17 plates were not seriously affected by corrosion. No signs of active mass shedding were visible. However, part of the PAM had penetrated into the pores of the gauntlets forming a thin film, the interior of the AGM being clean and white. No short circuits were observed. The tubes had soft and hard zones on touching. The structure of these two types of PAM zones was examined and it was established that softening of the PAM in these zones (i.e. disintegration of the skeleton structure) was the reason for the decline in battery power

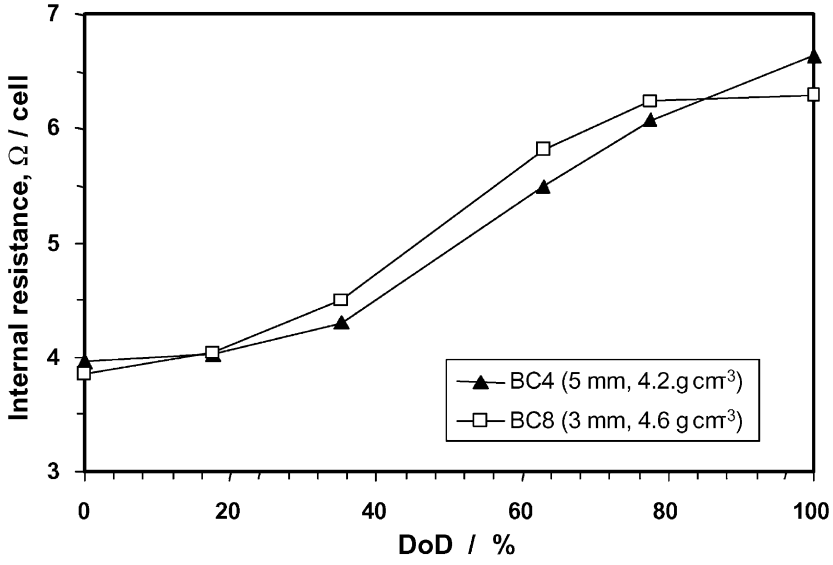

Fig. 16. Internal resistance at HCP vs. DoD of the batteries BC4 and BC8.

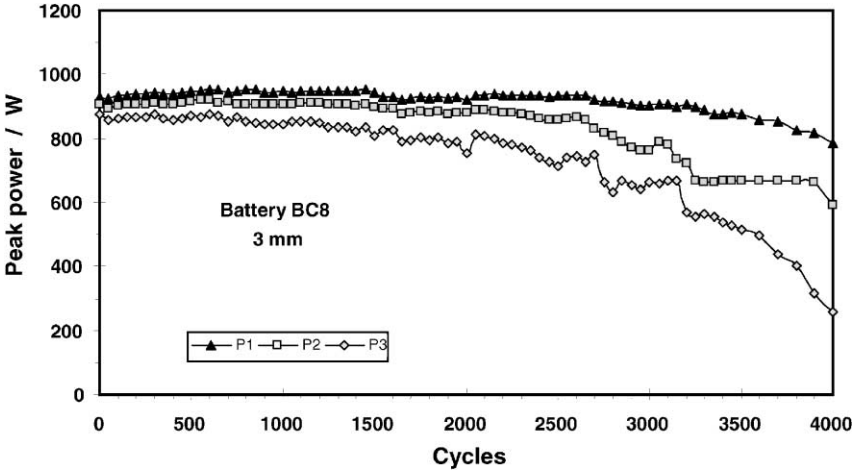

Fig. 17. Peak power changes on cycling battery BC8.

output. So it is important to slow down the degradation of the PAM macrostructure and to find methods to restore this structure after its degradation (softening). As the tubes maintain the volume of the PAM unchanged, it is essential to control the degradation of its structure and thus improve the cycle life of the battery.

3.2.3. The influence of pulse charge currents on specific energy, life and charging time of advanced tubular EV battery designs

Fundamental investigations of pulse charging were carried out and the influence of the pulse charge current investigated for flat plate grid, conventional and improved tubular designs. Results obtained showed that pulse charging did not give so much benefit as did fast charging and did not support capacity stability during cycling. Therefore the work was focused on modified constant current charge profiles, including IR compensated charge, combined with pulse charge for the final charging period.

Two types of battery, with advanced positive tubular plates, were manufactured by CMP using technology similar to that reported in Section 3.2.1. Type A was filled with acid of gravity of 1.30 g cm^{-3} and type B with 1.32 g cm^{-3}. The basic design of the 12 V battery blocks in both cases was a 13-plate configuration per cell with a nominal capacity of 70 Ah.

Some type A batteries were submitted to fast charge operation and these were labeled type F. In Table 3 the results of the capacity tests are shown for the two different battery types (A and B) at different discharge rates. The data refer to a 120 V string.

Based on single cell investigations, a current step down charge profile with correlating voltage limitations was developed and optimized. The voltage limitations for each current step take into account the voltage losses caused by internal resistance and also, polarization caused by the concentration gradient. Optimization of this current step profile was done with respect to charge time, temperature development during charge and gas evolution during charge. Fig. 18 shows an example of the curves for the cell voltage, the current, temperature, gas emission and SoC for the fast charge profile optimized for a single charge episode of battery type A.

Since the temperature increase for fast charge is significant, the different voltage limitations are temperature compensated. As the temperature was measured outside the cell (temperatures inside are expected to be significantly higher, in particular during the short time of fast charge) a rather high temperature compensation coefficient of −4 mV/K was used for the batteries.

The charge starts with a pre-current step of 150 A (about 2 C). This current step is necessary, because the cell shows something akin to an activation (voltage decreases initially with charge time), particularly after the cell has been fully discharged. Final C_5 (14 A) current pulses are applied in order to increase the final value of SoC.

Fig. 18 shows that a fairly high SoC can be achieved within a reasonable time, but it takes a long time for the final stages of charging to be completed. From a practical point of view, an EV will be used several times during a day and an extension of the daily driving range can be achieved by fast

Table 3
Performance summary for battery strings tested at ZSW

70 Ah (C_5) battery	Type A, 1.30 g cm^{-3}	Type B, 1.32 g cm^{-3}
$C_{5/5}$ discharge	71.2 Ah 28.5 Wh kg^{-1}	76.0 Ah 30.5 Wh kg^{-1}
$C_{5/2}$ discharge	61.1 Ah 24.1 Wh kg^{-1}	67.9 Ah 26.8 Wh kg^{-1}
$C_{5/1}$ discharge	53.7 Ah 20.7 Wh kg^{-1}	59.2 Ah 22.8 Wh kg^{-1}
ECE-15 discharge	53.29 Ah 19.81 Wh kg^{-1}	54.06 Ah 20.32 Wh kg^{-1}
ECE-15L discharge	67.5 Ah 26 Wh kg^{-1}	67.8 Ah 26 Wh kg^{-1}

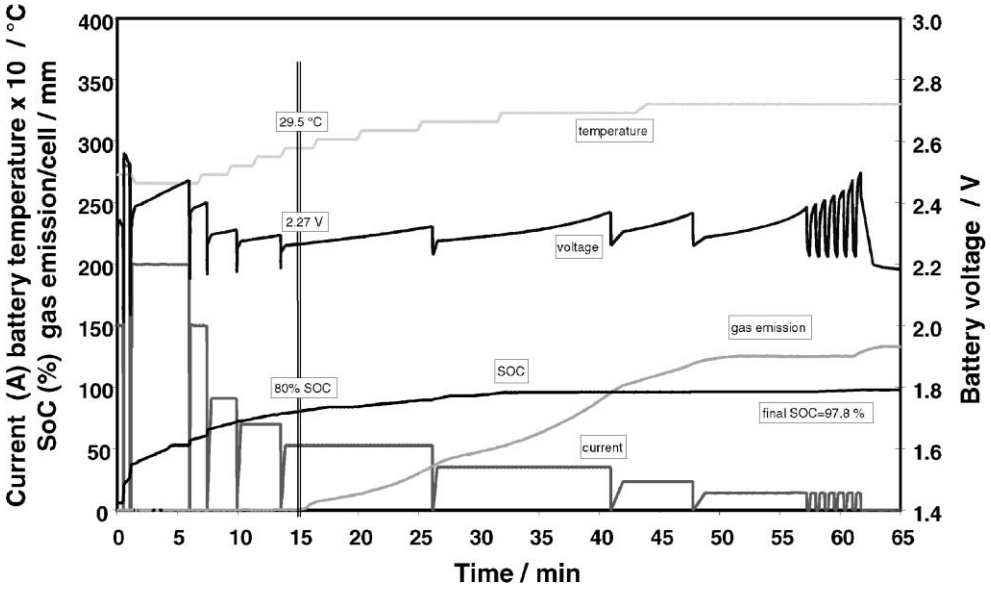

Fig. 18. Current, voltage, SoC, gas emission and temperature during fast charge by a current step profile (maximum current 4 C) optimized for the CMP type A battery.

charge. During the night there will be no need for fast charge. There will be enough time for conventional charge giving the chance for complete recharge of the battery and some equalization.

After installation, 8 pre-cycles (conditioning cycles) were carried out for each string as follows:

- discharge: $C_5 = 14$ A for 225 min (52.5 Ah = 75% DoD) and
- charge: $C_5 = 14$ A for 165 min (38.5 Ah) and 4.2 A with voltage limit 2.66 V/cell for 400 min rest time was 12 h.

After pre-cycling, an initial parameter test was carried out for each string. Thus, before life cycling started, for each string about 20 cycles had already been carried out.

According to the EUCAR test procedure, the initial useful ECE-15L capacity has to be determined three times after the short parameter test. The results of the initial ECE-15L useful capacity determination are listed in Table 4.

For string F, two weak blocks were indicated and were exchanged for new pre-cycled blocks. The initial determination of the useful ECE-15L capacity was repeated. As the useful capacities for string A and B were very close, the same average value was used for both strings and the 80% value for the limit in the ECE-15L 80% DoD life cycle test was set to 54.2 Ah. In order to carry out the tests under identical conditions and as the batteries are of the same type, the same 80% DoD value of 54.2 Ah was used for the life cycle test for string F.

The charge procedure (as also used for the parameter test and the determination of the initial ECE-15L useful capacity) has the following *IUI* charge.

1. Charge $0.4C_5 = 28$ A, voltage limitation 2.375 V/cell until current falls below: 1.6% $C_5 = 1.12$ A.
2. Charge at 1.5% $C_5 = 1.05$ A for 160 min (4% $C_5 = 2.8$ Ah).

The resulting charge factor increased relatively fast during cycling, so the charge regime was modified to limit the charge factor to 1.04.

For all strings a capacity check at C_5 discharge with *IUI* charge was carried out every 50 cycles, resulting usually in a recovery of the string (for few cycles). The ECE-15L cycle life criterion indicates that if the capacity drops three times below the 75% level of initial ECE-15L capacity, this equates to end of life. Table 5 shows the number of cycles achieved for each of the three battery types.

Comparing these results with previous experience of EUCAR ECE-15L testing and the tests in task 9 of the previous Brite-Euram project, only rarely does a lead acid

Table 4
Useful capacity during ECE-15L discharge cycle

	String		
	A	B	F
1 ECE-15L	67.09 Ah	68.05 Ah	58.3 Ah
2 ECE-15L	67.75 Ah	67.8 Ah	57.9 Ah
3 ECE-15L	67.75 Ah	67.4 Ah	57.7 Ah
Average useful capacity	67.75 Ah		58 Ah (two blocks exchanged)
Average specific energy	26 Wh kg^{-1}	26 Wh kg^{-1}	22.3 Wh kg^{-1}
1+			59.0 Ah
2+			66.9 Ah
3+			59.4 Ah
Average useful capacity			62.4 Ah
Average specific energy			23.8 Wh kg^{-1}

Table 5
Number of cycles achieved (taking into account the recovery with the capacity check)

	75% criteria
String A (filling acid 1.3 g cm^{-3})	161
String B (filling acid 1.32 g cm^{-3})	131
String F (filling acid 1.3 g cm^{-3})	137

battery last longer than about 130 cycles with this test regime. For the Hawker Genesis batteries tested in task 9 under a good charge condition, around 220 cycles were obtained. Thus these CMP tubular batteries have reached almost the same range as for these previous tests and any benefit in life might be observed in a real EV application where lead acid batteries have been shown to give good service despite poor ECE-15L test results.

Fig. 19 shows the ECE-15L capacity just before the parameter check and the capacity measured during the third C_5 capacity check. It is normally the case that the high current discharge capacity and the driving cycle capacity decrease faster than the lower current capacity. Fig. 19 shows, however, that for strings A and B the decrease in ECE-15L capacity and the decrease in C_5 capacity are quite similar. However, for the fast charged string F there is a similar decrease in ECE-15 capacity as for strings A and B, but the low current C_5 capacity is significantly more stable.

It should be mentioned that the performance of these batteries may have been impaired by the same delay in processing referred to in Section 3.2.1. The ultimate performance capability of batteries of this type, subjected to the procedures outlined here, may be stronger than was seen during this work.

3.3. Improvement in negative-plate performance

In hybrid and electric vehicle applications, a very high performance is required from the active materials in the battery, both during charge and discharge. In recent times, with the emphasis on premature capacity loss, more importance has been placed on studies of the positive plate rather than the negative. However, there are indications that, at high rates of discharge, and at the elevated temperatures expected in such duty, battery performance is limited by the negative plate.

The main objectives of this final phase of the program were to:

- investigate the nature of the phenomena leading to degradation of the structure of the NAM dependent on the mode of battery operation;
- investigate the influence of the expander on the degradation of the NAM structure;
- characterize thoroughly the expander materials, using advanced electrochemical and analytical techniques, so that it will be possible to follow their activity changes under different working conditions;
- investigate, in electrical tests, the characteristics and performance of the NAM, first in plate group assemblies and then in batteries and
- find an optimized expander formulation for the negative plates of VRLA batteries for EV applications.

3.3.1. Survey of expander materials and negative-plate formulations

Several electrochemical characterization techniques for expander materials were developed, optimized and applied

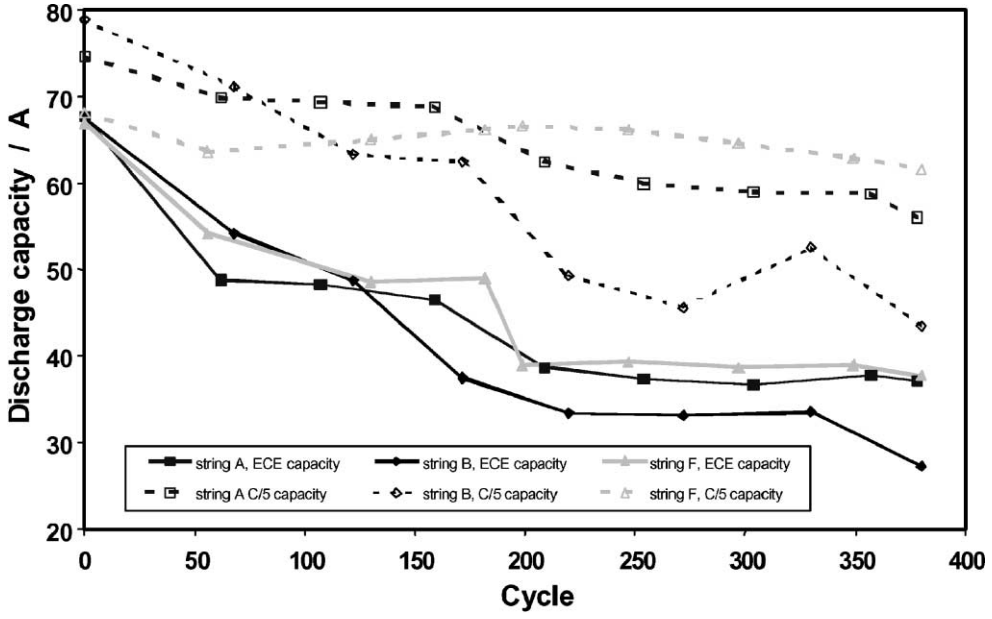

Fig. 19. Development of ECE-15L capacity prior to the capacity check and the C_5 capacity after the capacity check.

to a total of 19 potential expander candidates, including both natural substances and synthetic products. From the results obtained with these electrochemical techniques, the seven most effective additives were selected for further testing in real VRLA cells. These additives were: N17, DD8, DD5, S-004, VAN, Kraftplex and UP-414.

Subsequently, different negative formulations for testing in VRLA cells were defined. These included each one of the above-cited expanders at a fixed concentration, as well as several additional experiments with alternative concentrations of either the expander, carbon black or barium sulfate for the most promising candidates. The cells were formed and their initial performance obtained at different rates, as well as under the ECE-15L regime.

A motorcycle-type battery (size 12 V/15.0 Ah), was chosen to carry out the cell tests. This design was chosen due to the intermediate size of the batteries, which allowed the assembly of an appropriate number of single cells with just one paste mixing. The formulation used is shown in Table 6. The duration of the mixing process was approximately 30 min. Following this, the density of the active material was measured, resulting in a wet mass density of about 4.2 g cm^{-3} (with slight variations from test to test, depending on the expander) and values of plasticity and penetration adequate for manual pasting.

After the manual pasting process, the plates were subjected to a typical curing process in a laboratory curing chamber. This process was the following:

- 24 h at 55 °C and 100% relative humidity and
- at least 6 h at 60 °C and 20% relative humidity.

Thus, the following test formulations were evaluated:

1. 0.2% DD5;
2. 0.2% DD8;
3. 0.2% Kraftplex;
4. 0.2% N17;
5. 0.2% S-004;
6. 0.2% UP-414 and
7. 0.2% VAN.

These reference formulations (i.e. including the organic at the 0.2% level) are referred to as formulation A. In addition to these tests, three of the expanders (DD5, N17 and VAN) were selected for additional testing with the following variations.

- Tests 8–10: increase the expander concentration to 0.4% (formulation B).
- Tests 11–13: increase the carbon black concentration to 0.56% (formulation C).
- Tests 14–16: reduce the barium sulfate concentration to 0.5% (formulation D).
- Test 17: increase the carbon black concentration to 2.8%, i.e. 10 times higher than in the reference formulation (only for VAN) (formulation E).

Table 6
Formulation used in the reference formulation (formulation A)

Component	Amount	Concentration (related to oxide) (%)
Lead oxide	10 kg	100
Total water	1.350 kg	13.5
Sulfuric acid ($d = 1.40$ g cm^{-3}	0.84 kg	8.40
Fiber	7 g	0.07
Carbon black	28 g	0.28
Barium sulfate	100 g	1.00
Expander	20 g	0.20
Total	12.3 kg	

After the mixing process, the active mass was manually pasted onto Pb−Ca grids. The different amounts of components were chosen so that a limitation in the negative active mass was ensured. The following cell design was used:

- two positive plates per cell with 73 g positive formed mass per plate and
- one negative plate per cell with 50 g negative formed mass per plate.

The plates were carefully selected in order to have the same mass and grid weight throughout the different tests. In order to avoid too large an excess of acid, the rest of the void space inside the cell was filled with polypropylene spacers. The cast-on-strap welding was carried out using a manual welding device. Once the positive and the negative groups had been welded, the cells were inserted in the container and the cell lid was placed and sealed. Then, the formation process was carried out at a constant current of 0.55 A during 24 h, using thermostatically controlled baths at 45 °C and 130 ml/cell of 1.300 g cm^{-3} density formation acid.

After the formation of the cells, they were submitted to the designed plan of electrical tests. This plan was as follows.

3.3.1.1. Preliminary characterization tests. This test includes:

- discharge at 25 A (approximately 5 C);
- discharge at 10 A (approximately 2 C) and
- discharge at 5 A (approximately 1 C).

3.3.1.2. Initial tests previous to the ECE-15L cycling. The initial test has the following features:

- 5-h capacity (C_5);
- ECE-15L at 100% DoD;
- 5-h capacity (C_5);
- ECE-15L at 100% DoD;
- 5-h capacity (C_5) and
- ECE-15L at 100% DoD.

From the average capacity value of the three ECE-15L discharges at 100% DoD, both the useful initial capacity and the useful initial energy are calculated. These values served

to calculate the DoD in each cycle during the next cycling stage.

3.3.1.3. ECE-15L cycling at 80% depth-of-discharge (DoD). As a first stage of the electrical testing, a series of characterization discharges at different rates was initially carried out on the cells. The goal of these tests was to observe differences in the initial performance among all the groups tested at different discharge rates. Therefore, after formation, the cells were subjected to the following tests.

1. Discharge at 25 A (approximately 5 C) until a voltage lower than 1.0 V is obtained.
2. Recharge at 2.4 V per cell until 105% of the previous capacity has been recharged and then 2 h at 0.25 A (constant current).
3. Discharge at 10 A (approximately 2 C) until a voltage lower than 1.5 V is obtained.
4. Recharge (same as before).
5. Discharge at 5 A (approximately 1 C) until a voltage lower than 1.5 V is obtained.
6. Recharge (same as before).

Between three and six cells of each type were tested in every experiment at the cited rate, so that the values shown in the figures and tables correspond to *average values* over three or six cells for each test. One cell was monitored in each group using a cadmium reference electrode in order to assess which plate was responsible for the end of the discharge.

From the these experiments, the following general conclusions were drawn.

1. The cell design was correct: the negative plate was limiting the cell discharge.
2. The different expanders deliver up to about 10–13% different initial capacity at low rates (1 or 2 C). At higher rates (5 C), the differences become negligible.
3. Expanders DD5, DD8, and Kraftplex produce slightly better initial results than the rest of compounds.
4. For the three expanders which were tested varying the expander/carbon black/$BaSO_4$ content, it was found that, in general terms:
   - by increasing the expander loading from 0.2 to 0.4%, the initial capacity at low rates (1 C) is reduced, while no significant effect is found at high rates (5 C);
   - by increasing the carbon black loading from 0.28 to 0.56%, the initial capacity is not influenced at low rates, but it increases slightly at high rates. If this loading is further increased to 2.8%, there are no significant changes relative to the 0.56% level and
   - by decreasing the $BaSO_4$ loading from 1.0 to 0.5%, the initial capacity is more or less slightly reduced, depending on the expander.
5. In all cases, the extent of the respective effect depends strongly on the specific expander considered.

Following the preliminary testing, all the groups started the initial testing program under the ECE-15L specification for lead-acid batteries. According to this specification, the cells are submitted to a repetitive series of constant power charges, discharges and rest periods. The basic ECE-15L discharge unit is depicted in Fig. 20, where the power values have been calculated for the six-cell modules of the type used in this task. This basic unit is comprised of four sub-units, referred to as the 'urban part', performed successively, which have lower and shorter power peaks, and one additional sub-unit, referred to as the 'sub-urban part', with higher and longer power peaks. These five sub-units are executed consecutively, and they form the basic ECE-15L unit. Before the cycle life testing, the initial tests described in Section 3.3.1.2 were carried out. From the standard discharge tests, the average initial C_5 values were obtained, and, from the ECE-15L tests at 100% DoD, the average initial capacity and energy values at this regime were

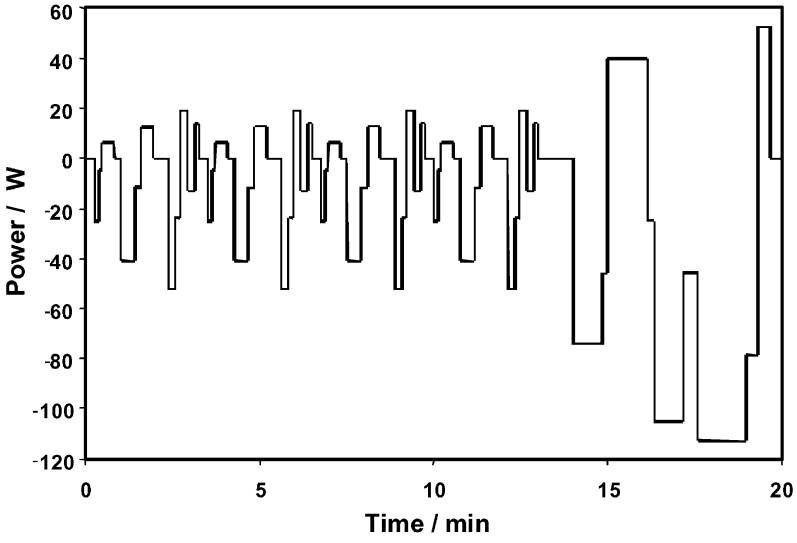

Fig. 20. ECE-15L cycling profile–profile of applied power for a six-cell module.

obtained. The ECE-15L cycle life tests were carried out by repeating the basic ECE-15L unit until the cells failed by reaching the lower voltage limit (1.5 V per cell). Typically, the failure in the test occurred during the high power discharges applied in the course of the sub-urban part of the ECE-15L unit.

3.3.1.4. Expanders at 0.2% concentration (formulation A). For the tests of the initial discharges for expanders using formulation A, it was found that, except for DD5, in all cases the capacity value ranged between 6 and 7 Ah, with rather small deviations from test to test. This remained the case even taking into account that the three tests were carried out alternately with a quite different kind of discharge test (the ECE-15L profile). By comparison with the preliminary characterization tests, DD8 and Kraftplex again showed a slightly better performance than the rest of expanders.

On the other hand, the results of the initial ECE-15L discharges at 100% DoD showed a different tendency. Under this EV regime, the initial capacity of all the expanders was around 5.5 Ah, and usually this capacity value was maintained quite constant in the second discharge, but in nearly all cases, at the third discharge a marked decrease in capacity was observed. This decrease was even more clearly observed in the discharged energy. From the first to the third test, there was a marked decrease in performance under the ECE-15 regime, amounting to around 15–20% in Wh. Clearly, this decrease was more closely related to the power requirements of the ECE-15L regime, and its influence on the present cell design, than to the real conditions of the cells. This is inferred since the C_5 tests, which are carried out alternately with the ECE-15L discharges, maintained their values in a quite constant manner.

3.3.1.5. Expanders at 0.4% concentration (formulation B). The average values produced by the three expanders tested using formulation B, in comparison to formulation A, can be found in Figs. 21–23.

After this work, the cell modules were subjected to the ECE-15L cycling test at 80% DoD. The overall results are complex and the conclusions depend quite heavily on the specific expander considered. Nevertheless, several general points can be made as follows.

- The best expanders (at the 0.2% level), in the cycle life test according to the ECE-15L specification, are: DD8, Kraftplex, and VAN.
- An increase in expander concentration from 0.2 to 0.4% may increase or decrease the ECE-15L cycle life, depending on the specific expander.
- An increase in carbon black concentration from 0.28 to 0.56% usually improves significantly the ECE-15L cycle life. In the case of VAN, if this loading is additionally increased up to 2.8%, the cycle life behaviour is further markedly enlarged.
- A decrease in $BaSO_4$ concentration from 1.0 to 0.5% adversely affects the cycle life performance.
- At the end of the ECE-15L cycling, the C_5 capacity is still >80%, but the ECE-15L capacity is poor. This suggests that the power requirement asked by the ECE-15L specification seems to be too hard for this cell design. In other words, the power requirements of the specification are influencing the results of the tests.

As a final result of the cited tests, the following formulations were selected for further testing in VRLA batteries of the orbital spirally-wound design:

- VAN at 0.2% concentration (control);
- VAN A at 0.2% concentration + increased carbon black concentration;
- DD8 at 0.2% concentration and
- Kraftplex at 0.2% concentration.

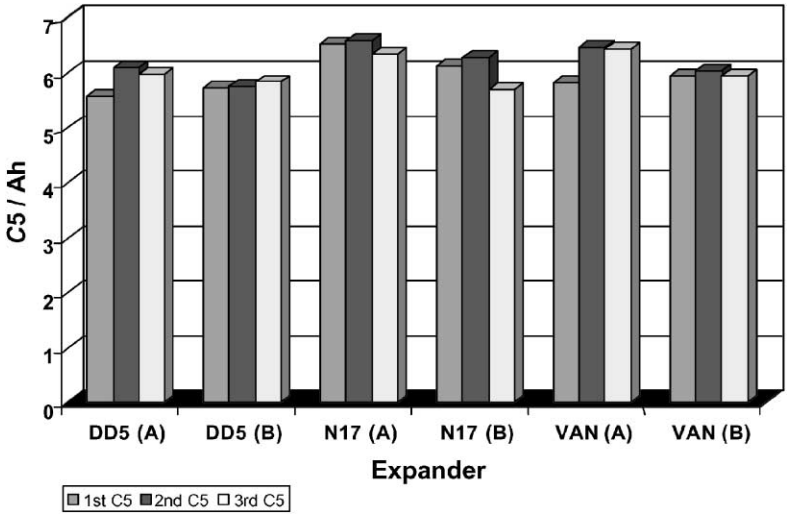

Fig. 21. Comparison of formulations A and B: C_5 initial capacities.

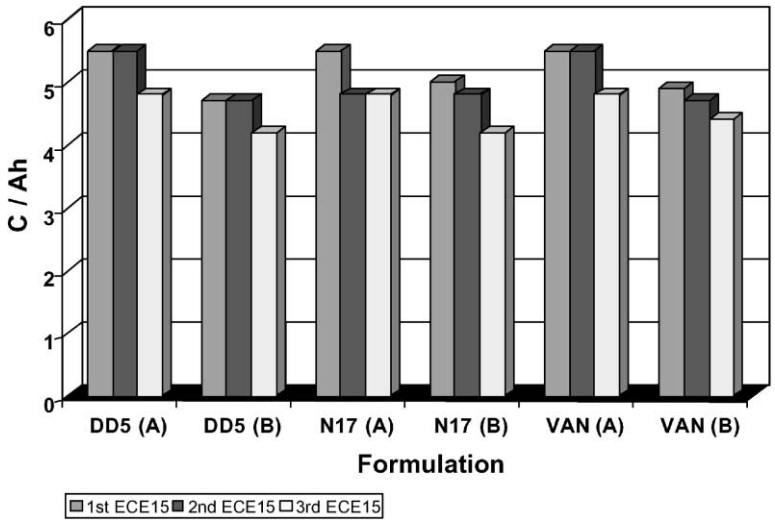

Fig. 22. Comparison of formulations A and B: ECE-15L (100% DoD) initial capacities.

Four batches of VRLA Orbital prototypes were manufactured in order to study the behaviour of the selected expanders, using the optimized concentration of 0.2% (versus dry lead oxide), as well as the improved concentrations of barium sulfate and carbon black. A control group of batteries, defined as N1, was manufactured using 0.2% of VAN as expander. A second batch, with 0.2% VAN plus 1% of carbon black were identified as N2. The other expanders tested were 0.2% Kraftplex (N3) and 0.2% Kraftsperse DD8 (N4).

In order to carry out a preliminary characterization of the prototypes, three modules of each batch were submitted to initial tests according to the EN 60095-1 specification. No significant differences were found in capacity values or cold cranking performance, but there were large differences in the values of charge acceptance as can be seen in Fig. 24.

Synthetic expanders like Kraftsperse DD8, and especially Kraftplex, clearly polarize the battery voltage to more negative values, reducing charge acceptance of the batteries under the conditions tested. These results were expected due to the strong polarization effect shown in the cyclo-voltammetric and other electrochemical tests previously carried out [3].

Before starting the ECE-15L life cycle testing, the useful capacity and the useful energy were determined. The results of the initial C_5 and ECE-15L discharges at 100% DoD, are represented in Table 7, and offered very similar values in useful capacity and useful energy for all the groups tested. An average value of 36.6 Ah in the 100% DoD profile was obtained as useful capacity. Therefore, the 80% DoD in the ECE-15L cycle life test were carried out up to 29.3 Ah.

Once the previous discharge program was completed, the cell modules started the ECE-15L life cycle test at 80% DoD. According to this profile (defined as a macro cycle), the batteries are discharged first to 40% DoD, then a rest

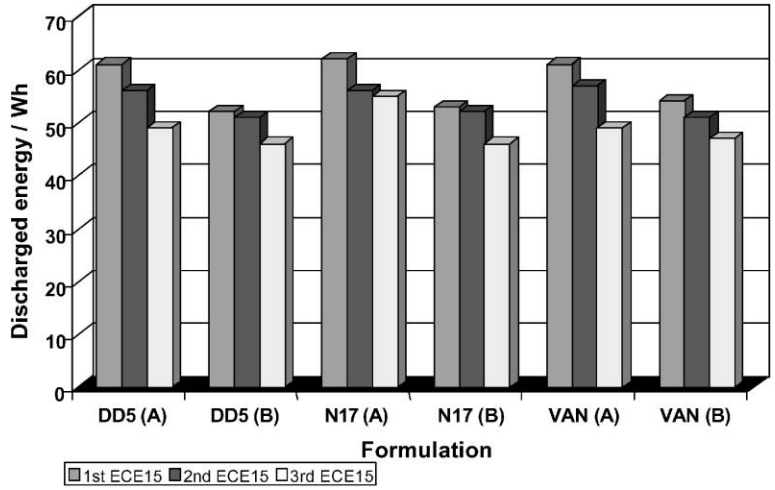

Fig. 23. Comparison of formulations A and B: discharged energy.

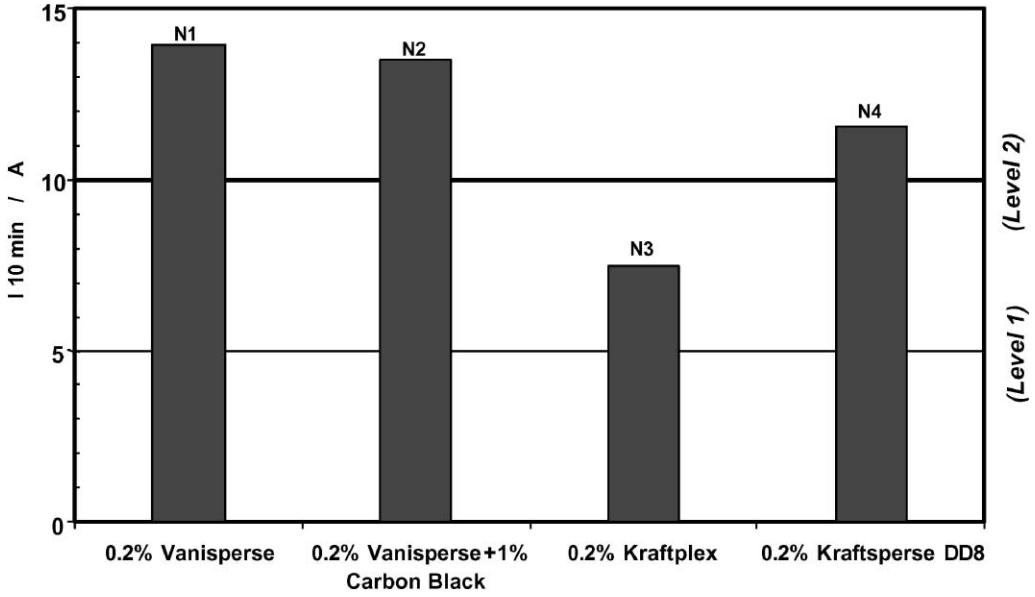

Fig. 24. Charge acceptance values.

period of 30 min is introduced, and finally the discharge continues up to 80% DoD. This is followed by a rest period of 1 h, a charge of 100% of the Ah previously discharged + 2 h at 1 A, and a final rest period of 1 h.

Every 50 μm cycles (or unit), a C_5 capacity control was carried out to check the health of the batteries. The evolution of the four groups of prototypes during the life cycle test can be seen in Fig. 25. It is interesting to compare these results with those obtained previously when testing the expanders in the VRLA prismatic 2 V cells. The best results were observed using Kraftplex DD8 and VAN at 0.2% concentration, but only 30 ECE-15L cycles were obtained. Although an increase of carbon black substantially improved the cycle life (about double number of cycles using VAN as expander), the prismatic configuration again showed a limitation when submitted to this ECE-15L specification. However, the orbital configuration offers a dramatic improvement of the ECE-15L cycle life, as the batteries have reached between 600 and 750 cycles. It should be noted that these ECE-15L results were obtained without restricting the temperature of the batteries to 23 °C.

3.3.2. Characteristics, performance, and degradation mechanisms of negative-plate active material

The structure of the active material of the negative plate consists of a skeleton of interconnected lead crystals and individual lead crystals grown over the skeleton. The individual lead crystals participate in the charge–discharge processes and form the energetic structure of the NAM.

On cycling, the lead branches of the skeleton are gradually converted into crystals of the energetic structure, or the crystals of the energetic structure may be converted into those of the skeleton, which limits the cycle life of the plate. This conversion depends on both the mode of battery operation (rate and mode of charge and discharge) and on the activity and stability of the expander(s) used. Because of the specific conditions of EV battery operation (high rates of charge and discharge, pulse discharge, etc.), it is important to investigate the nature of the phenomena leading to degradation of the structure of the NAM. It is also important to investigate the influence of the expander on this degradation of the NAM structure.

Table 7
C_5 and ECE-15L 100% DoD (initial cycling)

Prototype	First C_5 (10 A)	First ECE-15L 100% DoD	Second C_5 (10 A)	Second ECE-15L 100% DoD	Third C_5 (10 A)	Third ECE-15L 100% DoD
N1 (Ah)	41.2	36.2	40.4	36.1	41.0	36.5
N1 (Wh)		427		426		433
N2 (Ah)	41.9	36.8	41.4	36.5	42.0	37.0
N2 (Wh)		435		432		439
N3 (Ah)	42.0	36.8	41.7	36.5	42.4	37.1
N3 (Wh)		434		432		439
N4 (Ah)	42.2	36.9	41.6	36.6	42.0	37.1
N4 (Wh)		436		432		439

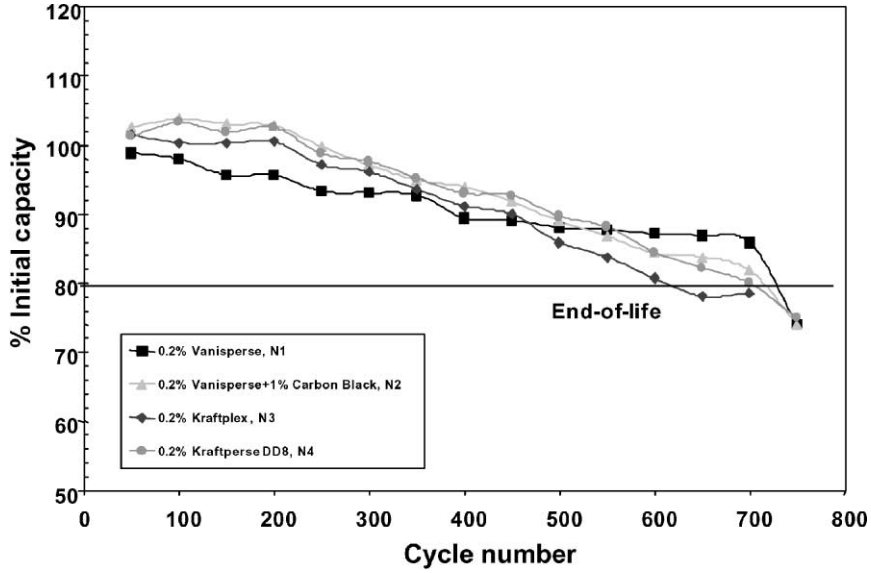

Fig. 25. Evolution of C_5 capacity for each 50 μm cycles.

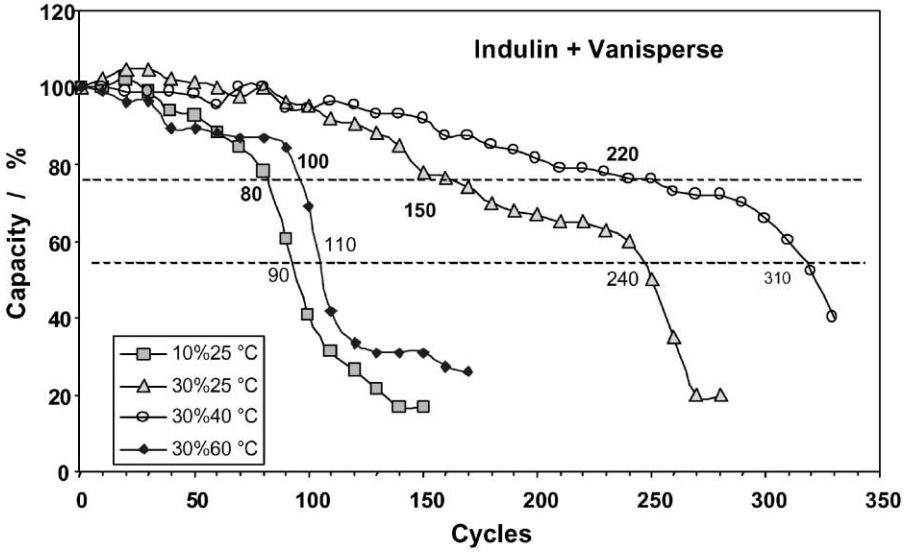

Fig. 26. Capacity changes on cycling of the cells with a blend of In and VAN.

In VRLA batteries the expander contained in the negative active mass is subjected to oxidation by the evolved oxygen that takes part in the recombination process. Also, the batteries for EV applications operate at high temperatures and under conditions of high current pulse discharge, which have a highly aggressive influence on the expander. Therefore, to find chemically stable expanders that would operate well at high temperatures is a problem of the utmost importance for EV batteries.

A series of battery tests were performed with negative plates prepared with a blend of In and VAN. These cells were subjected to cycling tests following the ECE-15 test protocol described above at 25% utilization of the negative active mass. The battery test parameters are summarized in Table 8.

The results of the ECE-15 tests of cell 11–14 are presented in Fig. 26. The figure shows the relative ECE capacity of the cells determined as the ratio between the discharge capacity on ECE-15 cycling and the useful ECE capacity, which is the average capacity of the first 3 ECE cycles. The ECE-15 test

Table 8
Battery test parameters

Battery number	Expander type	Compression (%)	Test (°C)
11	Indulin + Vanisperse	30	25
12	Indulin + Vanisperse	10	25
13	Indulin + Vanisperse	30	40
14	Indulin + Vanisperse	30	60

Table 9
Paste parameters

	Negative paste number 10		Negative paste number 11		Positive paste	
	Amount	(%)	Amount	(%)	Amount	(%)
Leady oxide (72% PbO) (kg)	4	–	4	–	8	–
Sulfuric acid (1.40 g cm^{-3}) (ml)	260	4.5	260	4.5	520	4.5
Water (ml)	440	11	440	11	860	10.7
UP-393 (g)	**8**	**0.2**	–	–	–	–
UP-414 (g)	–	–	**8**	**0.2**	–	–
$BaSO_4$ (g)	16	0.4	16	0.4	–	–
Carbon black (g)	8	0.2	8	0.2	–	–
Paste density (g/cm^3)	4.15	–	–	–	4.20	–

procedure assumes that the battery has reached its end of life when it fails to deliver 80% of its useful capacity.

The temperature exerts a very strong influence on the life of the batteries. On temperature increase to 40 °C the cycle life of the negative plates increases, but then at 60 °C it decreases abruptly. Probably, at this temperature the chemical stability of the expanders declines dramatically and their effect on the capacity of the negative plates almost disappears.

The curves in Fig. 26 show that the cells with low compression (10%) have a cycle life of 80 cycles. For the cells with 30% compression, when cycled at 25 °C, have a cycle life of 150 cycles and the best cycle life performance, about 220 cycles, is exhibited by those cells cycled at 40 °C. Those tested at high temperature (60 °C) last only 100 cycles before reaching their end of life.

Tests were also carried out with cells prepared with expanders UP-393 and UP-414 supplied by Borregaard Lignotech. The conditions of paste preparation and their formulations are summarized in Table 9. The cells were subjected to cycling tests following the ECE-15 test protocol at 25% utilization of the negative active mass. The test conditions are summarized in Table 10.

Table 10
Battery test conditions

Battery number	Expander type	Compression (%)	Test (°C)
15	UP-393	30	25
16	UP-393	30	40
17	UP-393	30	60
18	UP-414	30	25
19	UP-414	30	40
20	UP-414	30	60

The results of the ECE-15 tests of the experimental batteries with UP-393 expander are presented in terms of relative ECE capacity of the cells in Fig. 27. It appears that the cycle life of the cells tested at high temperature (60 °C) is about 140 cycles.

The cells cycled at 25 °C have a capacity within the range 70–80% of the useful capacity for about 300 cycles and these

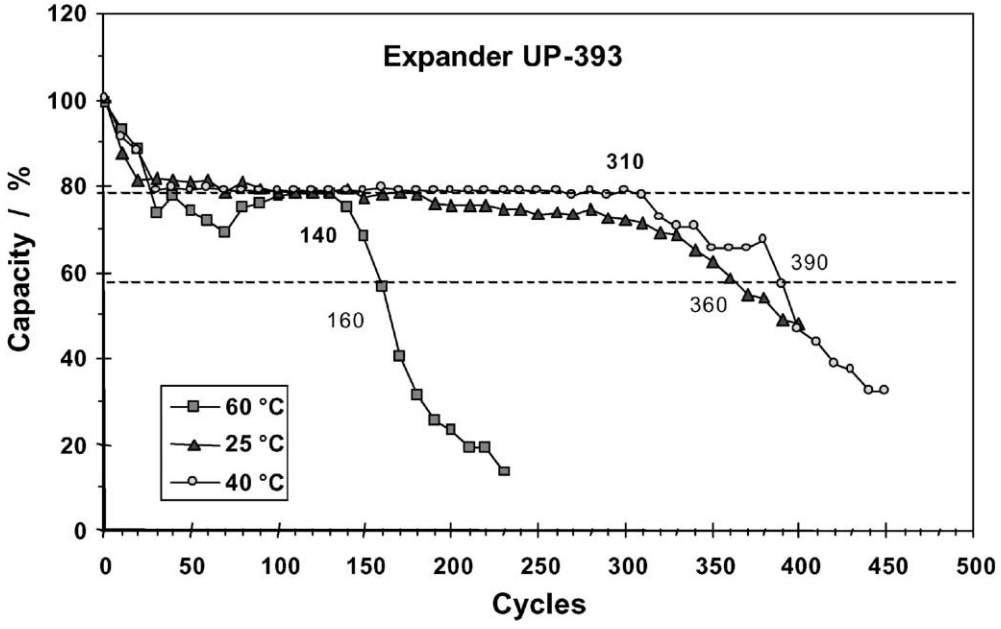

Fig. 27. Capacity changes on cycling of the cells with UP-393 expander.

cells reach their end of life after 360 cycles. At 40 °C, the relative capacity of the cells is about 80% for 310 cycles and begins to decrease thereafter.

On comparing the data in Figs. 26 and 27 it can be seen that the capacity of the negative plates prepared with expander blend In + VAN is between 95 and 100% of the useful capacity during the first 80–100 cycles and decreases thereafter, whereas the plates with expander UP-393 exhibit a decline in capacity performance down to 80% of the useful capacity within the first 15–20 cycles, but then this capacity is maintained for about 300 cycles. This peculiarity of the capacity behaviour is probably due to the nature of the expander used. During the first few cycles, expander UP-393 is probably transformed partially, under the action of hydrogen and potential, into a substance that keeps the structure of the negative active mass relatively unchanged throughout 300 cycles, but this structure yields lower plate capacity.

The question arises then whether the stationary capacity performance on cycling could be improved to values above 80% of the useful capacity and how? First, it was decided to investigate the influence of the charge mode. For this purpose, two identical cells with negative plates with UP-393 were subjected to ECE-15L cycling tests employing the following two different charge modes.

1. $I_1 = 0.4C_5$ up to $U_2 = 2.50$ V; $U_2 = 2.50$ V up to $F_{ch} = 108\%$.
2. $I_1 = 1.2C_5$ up to $U_2 = 2.5$ V; $U_2 = 2.5$ V, $F_{ch} = 108\%$; $I_3 = 0.1C_5$, $F_{ch} = 118\%$.

The results of this test are presented in Fig. 28. It is evident from the figure that the second charge mode improves the capacity performance of the plates by more than 10%. It follows then that the selection of battery charge mode should take into account the type of expander used.

The results of the ECE-15 tests of the experimental cells with UP-414 expander are presented in Fig. 29. In this case also, the cycle life of the negative plates tested at 60 °C is the shortest (120 cycles). Until cycle 160, the cells tested at 40 °C have the highest capacity, which however falls down below 80% of the useful capacity thereafter. The capacity of the cells cycled at 25 °C is constant and very close to 80% of the useful capacity for about 280 cycles and then begins to decrease.

These results indicate that the cells with expanders UP-393 and UP-414 have similar performance characteristics (capacity and cycle life) when cycled at 25 °C, but expander UP-393 is more stable than UP-414 at 40 °C and ensures the highest capacity at this temperature for 310 cycles.

In an attempt to investigate the efficiency of complex expanders batteries with three-component expander blends were produced, namely:

(a) In + VAN + UP-393 and
(b) In + VAN + UP-414.

All the component expanders were present at the 0.1% level. Again, the cells had a compression of 30% and were tested at 25, 40 and 60 °C. The cycling test results are presented in Figs. 30 and 31.

As in all other tests, here again the shortest cycle life (50–65 cycles) was observed with the negative plates cycled at 60 °C. When the tests were conducted at 25 and 40 °C, the negative plates with (In + VAN + UP-393) endured 180 and 190 cycles, respectively, against 145 and 175 cycles for the plates with (In + VAN + UP-414). The results indicate that the life of the plates with three-component expander blends is shorter by about 40–50% than that of their counterparts with single- and two-component expanders. In order to check whether the charge mode selected (118% charge factor) is not responsible for the above cycle life performance, three cells with negative plates produced with the three-component

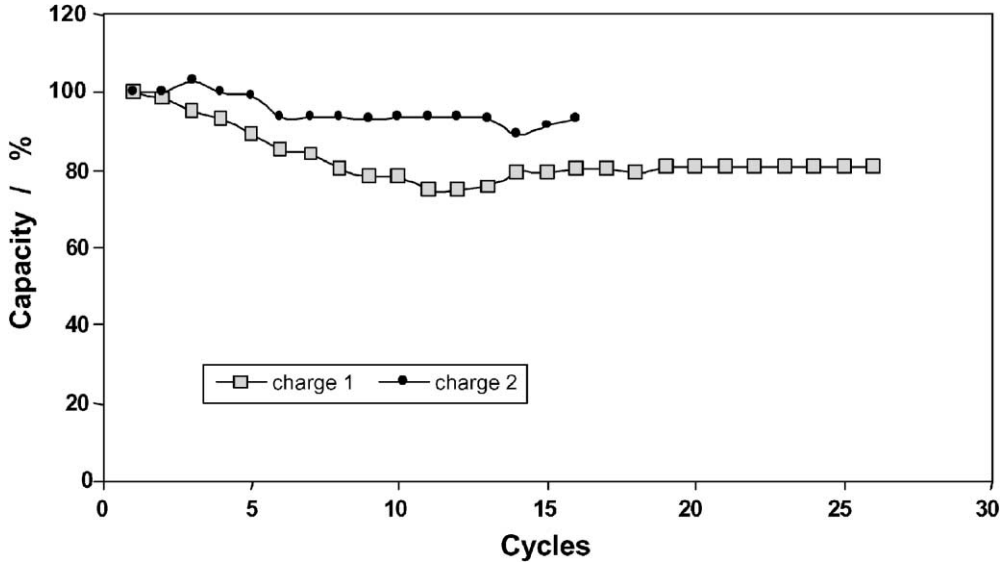

Fig. 28. Capacity changes during cycling with two different charge modes.

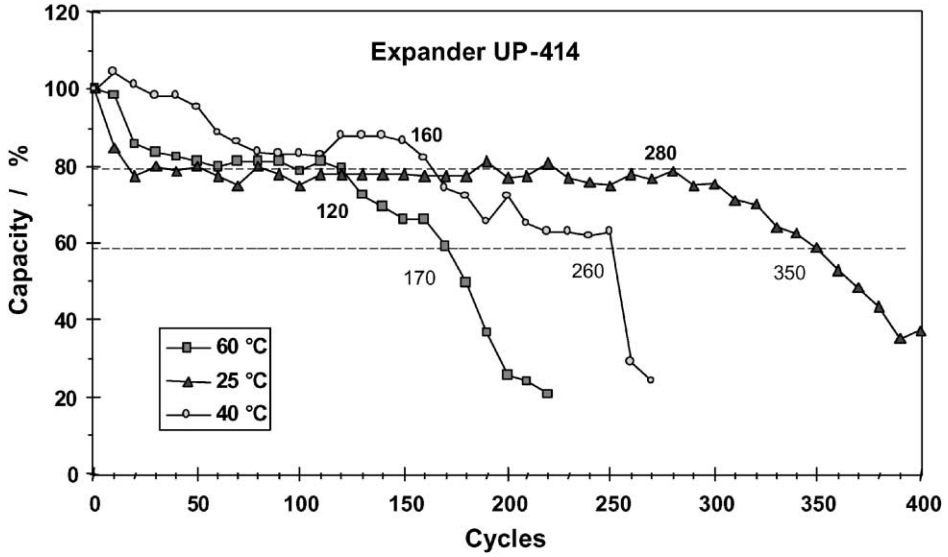

Fig. 29. Capacity changes on cycling of the cells with UP-414 expander.

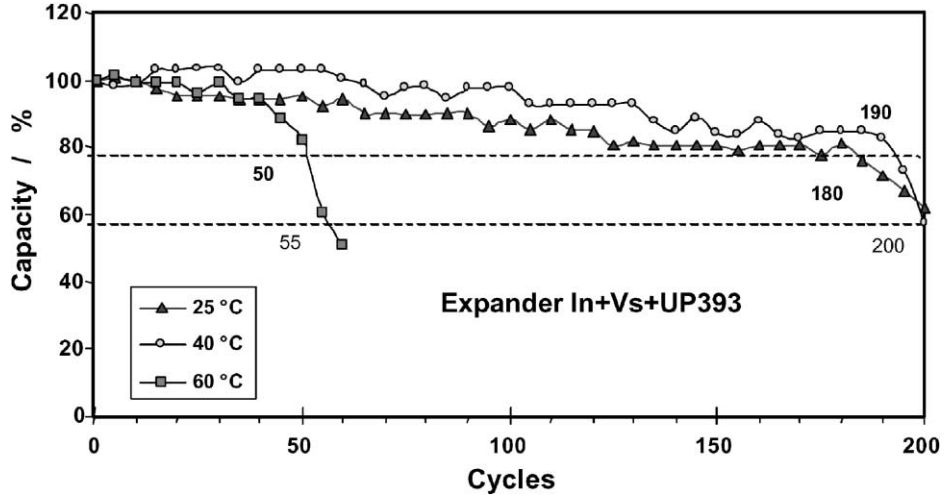

Fig. 30. Capacity changes on cycling the cells with a three-component expander blend In + VAN + UP-393.

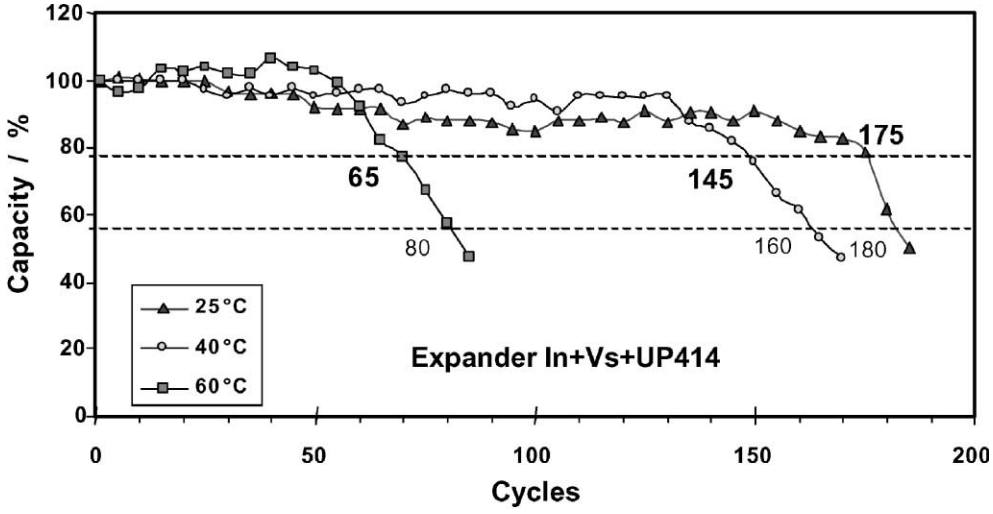

Fig. 31. Capacity changes on cycling the cells with a three-component expander blend In + VAN + UP-414.

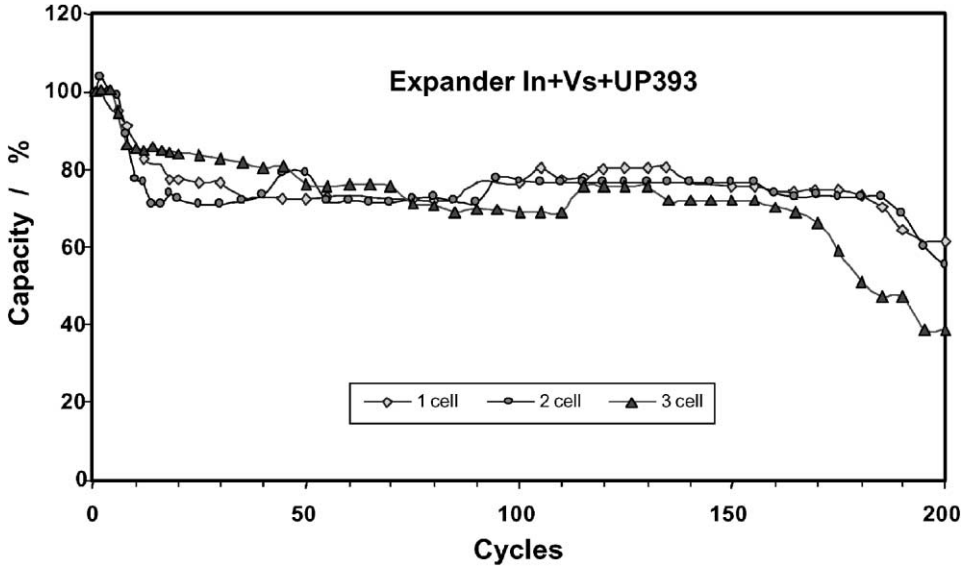

Fig. 32. Capacity changes on cycling of the cells with a three-component expander blend In + VAN + UP-393. Charge mode *IU* (108%).

expander blend (In + VAN + UP-393) were subjected to the same cycling tests (ECE-15L) employing the charging scheme used in the previous tests (*IU*):

$I_1 = 0.4C_5$ up to $U_2 = 2.50\,\text{V}$

$U_2 = 2.50\,\text{V}$ until $F_{\text{ch}} = 108\%$

The results obtained are presented in Fig. 32. As evident from the figure, the cycle life performance of the plates under this charge mode is similar (170–180 cycles) to when a considerable overcharge was applied (Figs. 30 and 31). Moreover, Fig. 32 shows clearly that the charge mode exerts a very strong influence on the capacity, and on the power output of the battery, under conditions of pulse charge (ECE-15), respectively. If the charge is subjected to a small overcharge (charge mode *IU* (108%)), the capacity of the negative plates declines rapidly at the beginning of cycling and then increases to reach about 80% of the useful capacity within the next 10–15 cycles and remains almost constant at this low level thereafter. If the charge is subjected to high overcharge levels (charge mode *IUI* (118%)), no initial capacity decline is observed.

Cells charged to higher overcharge levels deliver substantially higher energy throughout their cycle life. The results of this work indicate that the longest cycle life is observed with the negative plates prepared with the following expanders: UP-393, UP-414 and In + VAN.

The following results were obtained when the cycling tests were conducted according to the ECE-15 test protocol.

(a) Negative plates with UP-393 expander exhibit the longest cycle life.
(b) Batteries with In + VAN or UP-393 have similar behaviour on cycling; their life increases in the temperature range 25–40 °C and declines abruptly at 60 °C.
(c) Batteries with UP-414 have the best cycle life performance at 25 °C, but with increase in temperature the life of their negative plates decreases rapidly.
(d) On cycling at 60 °C expanders disintegrate and all types of batteries have almost the same cycle life, between 120 and 170 cycles.

It can be generally concluded from the above test results that UP-393 is the most appropriate expander for batteries cycled under the conditions of the ECE-15 test protocol. The second best expander for these battery applications is the blend In + VAN.

3.3.3. Electroanalytical measurements

The effect of expander materials, in connection with the electrochemical processes characterizing the behaviour of lead in sulfuric acid solutions, has been investigated at the Politecnico di Torino. This was done both by using small flat lead electrodes immersed in sulfuric acid solutions in which the expanders were dissolved and by using negative plates purposely prepared with the given expanders.

The work reported in the scientific literature on this subject, indicates the utmost importance of the adsorption process of the organic substances on the electrochemical active surfaces of lead. The adsorption process has a notable influence, not only on the kinetics for hydrogen evolution, but also on the crystallization and reduction of lead sulfate. All these processes exercise a strong influence on the self-discharge and on the so-called charge acceptance. Electrocrystallization of lead sulfate and its reduction are the phenomena which affect the possibility of maintaining the highly porous structure of the plates.

Initial electrochemical tests [3] provided information about the function of expanders and, helped in the ranking of their effectiveness under test, and hence the selection of

Table 11
Expander details

Sample	Expander	Batch reference
V1	Vanisperse A	8189 (1996)
V2		190951 (1998)
V3		191357 (2000)
K1	Kraftplex	1998
K2		2000a
K3		2000b
D1	DD5	1998
D2		2000a
D3		2000b

those chosen for further testing in batteries. Two different aspects have been proposed for further investigation: (i) comparison of the results obtained by three different electrochemical techniques on different batches of the same organic expander (i.e. batch-to-batch reproducibility) and (ii) electrochemical characterization of expander mixtures.

In the first part of this program, tests were performed on three different batches of various expanders as detailed in Table 11. The expanders were tested according to various electrochemical techniques, namely: (i) electrochemical impedance; (ii) potentiostatic transients and (iii) cyclic voltammetry.

Due to the variability of the measured data, several tests were carried out for each sample. Every test was recorded in the 'blank condition', before the addition of the expander and after addition. Values of the inter-phase capacitance C, and of the transfer resistance R were taken. The ratios Re/Rb and Ce/Cb of the values measured in the presence and in the absence of the expanders were also recorded.

An example of the current monitoring is reported in Fig. 33, where the trend of the change of the cathodic current after the addition of 40 ppm of expander is shown. In spite of the scatter of the experimental data, which can be ascribed to the difficulty of obtaining reproducible initial surface conditions of the lead electrode, interesting information is obtained by the comparison of the different sets of data for each expander. To illustrate the experimental difficulty related to the reproducibility of the measured data, Figs. 34–36 report the values of the Re/Rb ratio for all the tests performed on the different expanders.

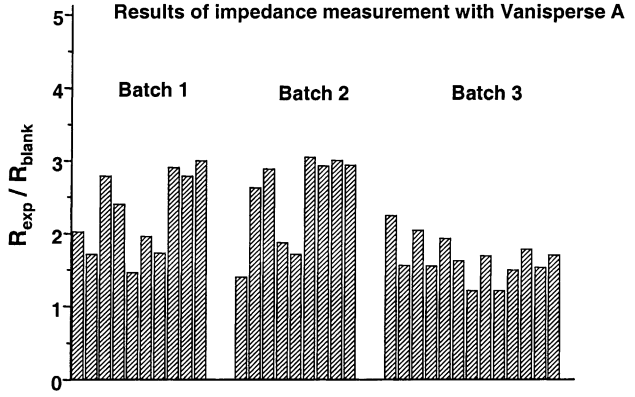

Fig. 34. Values of the Re/Rb ratio for the three batches of VAN (V1, V2 and V3).

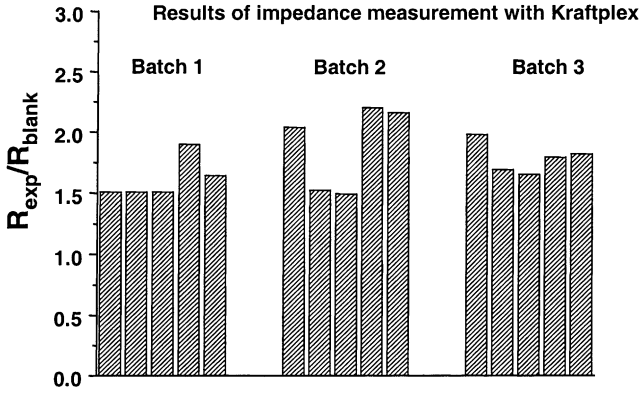

Fig. 35. Values of the Re/Rb ratio for the three batches of Kraftplex (K1, K2 and K3).

Two examples of the potentiostatic step data obtained are plotted in Fig. 37(a) and (b). Results obtained with cyclic

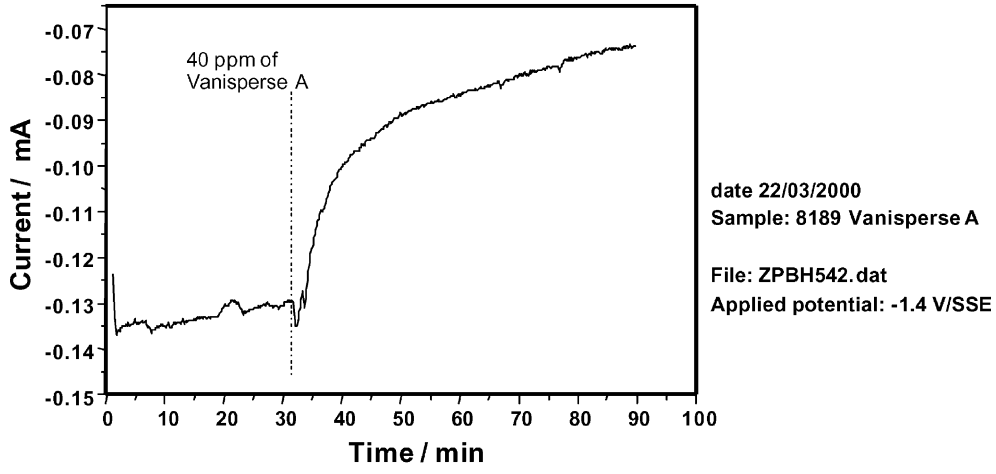

Fig. 33. Cathodic current variation with time during the test.

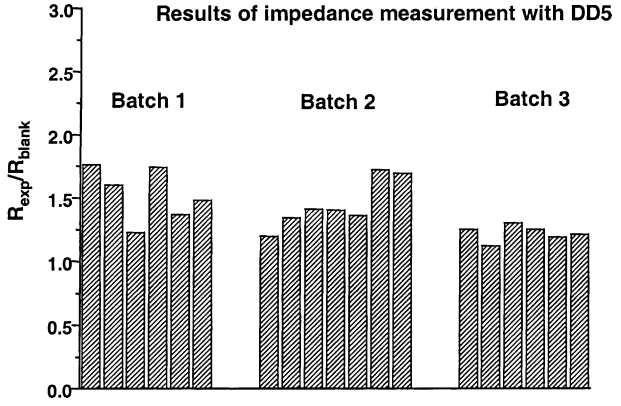

Fig. 36. Values of the Re/Rb ratio for the three batches of DD5 (D1, D2 and D3).

voltammetry, confirmed the findings with the other techniques as far as the different batches of expander are concerned. For DD5 and Kraftplex the three batches provide broadly similar results, even taking in to account the scatter of the experimental data. For VAN, again with batch 3 (sample 191357), the effectiveness is lower than that obtained with the other two samples. As far as the trend of the cyclovoltammograms is concerned, in all cases an increase in the anodic peak area was observed upon cycling. This increase was higher when the expander is present.

In the presence of the expander, the cathodic peaks were broadened and shifted. These features were similar to those reported earlier [3]. In all cases a very good agreement between the anodic and cathodic charges was obtained.In summary it can be said that:

(i) the electrochemical techniques used to characterize the organic expanders provide a means for laboratory evaluation of the expander's efficiency, but cannot be regarded at present as an analytical tool due to poor reproducibility of the experimental data. To overcome this difficulty, particularly when the scope of the investigation is a quantitative comparison of different expanders, a statistical treatment of the experimental results is required, based on a large set of tests (at least 10 runs of the same test);
(ii) the comparison of three different batches of the same organic revealed differences in behaviour and
(iii) characterization of expander mixtures to look for possible synergistic effects was initiated by preliminarily considering In/VAN 1:1 mixtures. All three electrochemical techniques showed higher performances for the mixtures than for the single components.

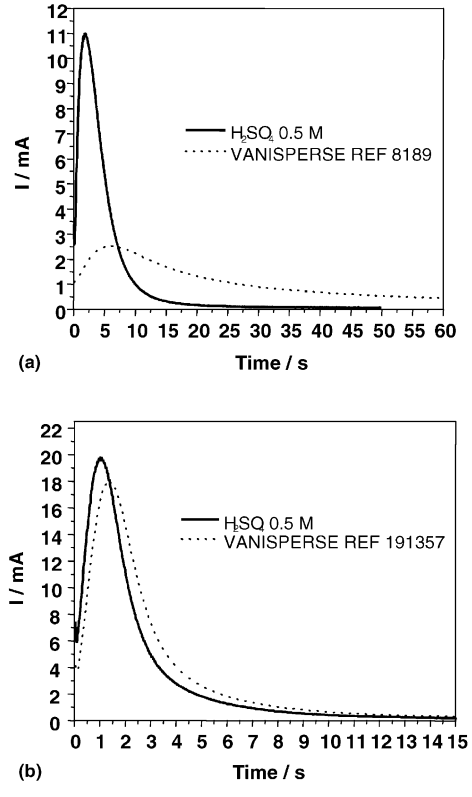

Fig. 37. Potentiostatic transients with sample (a) V1 and (b) V3 of VAN.

4. Conclusions

Some substantial conclusions may be drawn from the results of this extensive research program on the performance of VRLA batteries for EV duty.

4.1. Separators

Composite separator materials and separator blends show some promise for investing VRLA batteries with improved performance in deep cycle duty. In other tests, gel cells yielded highest discharge capacities but the high-silica material, AJS, provided longest life. It would also seem from the results of this task that the application of an external mechanical pressure reduces corrosion of the positive grid.

4.2. Tubular plate batteries

Cells constructed with thin pressure die-cast spines show promise of substantial improvements in specific energy over existing technology and tests of such cells yielded good cycle life. Batteries built to similar design did not perform so well and it is thought that this was due to defects in the build procedure used. These shortcomings may have influenced the results of fast charge studies of batteries with tubular positive plates. The performance of die-cut SGT positive plate batteries is sensitively affected by the mode of testing and by the charge factor.

4.3. Negative plate

Tests of a variety of negative-plate formulations appeared to show benefits of increased carbon loading. Results with flat plate cells tested according to the ECE-15L procedure gave short lives, but a spiral wound design gave up to 750 deep cycles. Different expanders appeared to give different

performance in the negative plate but there was evidence of considerable batch-to-batch variation, at least for VAN.

Finally, it should also be noted that work at CMP on factors limiting lead acid battery performance in ECE-15L testing has indicated that restricting the test to a battery temperature of 23 °C adversely affects the performance of the battery under this test regime. For this reason, in the work on the orbital battery, the battery was allowed to operate at its normal working temperature.

Acknowledgements

This work has been sponsored jointly by the European members of the Advanced Lead-Acid Battery Consortium and the European Commission under the Brite-Euram Program. Their permission to publish this paper is gratefully acknowledged. This summary of the work has been prepared from progress reports produced by the various researchers.

References

[1] A. Cooper, J. Power Sources 59 (1996) 161–170.
[2] T.G. Chang, D.M. Jochim, J. Power Sources 91 (2000) 177–192.
[3] A. Cooper, J. Power Sources 88 (2000) 53–70.
[4] K. McGregor, A.F. Hollenkamp, M. Barber, T.D. Huynh, H. Ozgun, C.G. Phyland, A.J. Urban, D.G. Vella, L.H. Vu, J. Power Sources 73 (1998) 65–73.